


THE UNIVERSITY OF MICHIGAN  
COLLEGE OF ENGINEERING  
Department of Aeronautical and Astronautical Engineering  
Aircraft Propulsion Laboratory

Quarterly Progress Report No. 3  
(1 December 1962 to 28 February 1963)

THE FEASIBILITY OF A ROTATING DETONATION WAVE ROCKET MOTOR



ORA Project 05179

under contract with:

AIR FORCE FLIGHT TEST CENTER  
6593d TEST GROUP (DEVELOPMENT)  
CONTRACT NO. AF 04(611)-8503  
EDWARDS AIR FORCE BASE, CALIFORNIA

administered through:

OFFICE OF RESEARCH ADMINISTRATION

ANN ARBOR

March 1963



## TABLE OF CONTENTS

	Page
LIST OF FIGURES	v
NOMENCLATURE - PART I	vii
FOREWORD	ix
SUMMARY	x
I. ANALYTICAL MODEL OF THE ROTATING DETONATION WAVE ENGINE	1
A. Introduction	1
B. The Complete Mixing Case	1
C. The No-Mixing Case	8
D. Similarity and Sizing Rules for the Internal Gas Dynamics of Rotating Detonation Wave Engines	13
E. Application of Similarity and the Sizing Rules to Preliminary Design	16
F. Results and Conclusions	17
II. EXPERIMENTAL STUDIES	19
A. The Gaseous, 100-lb Thrust Motor	19
B. Temperature and Pressure Effects on Hydrogen-Oxygen Detonation Velocities	
1. Introduction	
2. Test Equipment	21
3. Methods and Procedures	21
4. Test Results	22
5. Discussion of Test Results	22
C. Detonation through Heterogeneous Liquid-Gas Media	23
D. Geometrical Tests	26
III. STUDY PLANS FOR THE NEXT QUARTER	29
REFERENCES	30

EMM

JMK

1475

103

## LIST OF FIGURES

### Figure

- 1(a) Mach Number,  $M$ , as a Function of the  $B\eta$  Product for the Case of a Blocked Injector ( $d\bar{m}_P = 0$ )
- 1(b) Dimensionless Velocity,  $\bar{v}$ , as a Function of the  $B\eta$  Product for the Case of a Blocked Injector ( $d\bar{m}_P = 0$ )
- 1(c) Dimensionless Pressure,  $\bar{P}$ , as a Function of the  $B\eta$  Product for the Case of a Blocked Injector ( $d\bar{m}_P = 0$ )
- 2(a) Dimensionless Properties  $\bar{P}$ ,  $\bar{T}$ ,  $\bar{\rho}\bar{v}$ , and  $\mu$  as Functions of the Dimensionless Circumferential Coordinate,  $\eta$
- 2(b) Mach Number,  $M$ , and Dimensionless Velocity,  $\bar{v}$ , as a Function of the Dimensionless Circumferential Coordinate,  $\eta$
- 3(a) Pressure Profile of an  $H_2 - O_2$  Detonation Wave in a Straight Tube Using an Unmodified Kistler Pressure Transducer
- 3(b) Pressure Profile of an  $H_2 - O_2$  Detonation Wave in a Straight Tube Using a Modified Kistler Pressure Transducer
- 4 Wall Temperature Profile Behind an  $H_2 - O_2$  Detonation Wave in a Straight Tube Using a Nanmac Wall Thermocouple
- 5 Photographs of the Starting Sequence of the Gaseous, 100-lb Thrust Motor Obtained by a "Fastax" 8mm Framing Camera
- 6 Photograph of the Test Setup for the Measurement of the Temperature and Pressure Effects on Hydrogen-Oxygen Detonation Velocities
- 7 Schematic View of the Test Setup for the Measurement of the Temperature and Pressure Effects on Hydrogen-Oxygen Detonation Velocities
- 8 Photograph of the Coiled Detonation Tube and the Low-Temperature Vessel
- 9 Schematic View of the Ionization Probe
- 10 Schematic View of the System for Detonation Velocity Measurements
- 11 Experimental Detonation Velocity,  $U_D$ , of Hydrogen-Oxygen Detonations as a Function of the Mole-Fraction of Hydrogen ( $X_{H_2}$ ) from Data Obtained by Moyle (Reference 5)

## LIST OF FIGURES (continued)

### Figure

- 12 Experimental Detonation Velocity,  $U_D$ , of Hydrogen-Oxygen Detonations as a Function of the Initial Temperature,  $T_1$ , for  $X_{H_2} = 0.500$
- 13 Experimental Detonation Velocity,  $U_D$ , of Hydrogen-Oxygen Detonations as a Function of the Initial Temperature,  $T_1$ , for  $X_{H_2} = 0.667$
- 14 Experimental Detonation Velocity,  $U_D$ , of Hydrogen-Oxygen Detonations as a Function of the Initial Temperature,  $T_1$ , for  $X_{H_2} = 0.730$
- 15 Experimental Detonation Velocity,  $U_D$ , of Hydrogen-Oxygen Detonations as a Function of the Initial Temperature,  $T_1$ , for  $X_{H_2} = 0.800$
- 16 Experimental Detonation Velocity,  $U_D$ , of Hydrogen-Oxygen Detonations as a Function of the Mole-Fraction of Hydrogen,  $X_{H_2}$ , for Initial Pressure,  $P_1 = 10$  Atmospheres
- 17 Comparison of Experimental Detonation Velocity,  $U_D$ , as a Function of Initial Temperature,  $T_1$ , at Various Initial Pressures,  $P_1$ , with Results of Other Investigators for Stoichiometric ( $X_{H_2} = .667$ )  $H_2 - O_2$  Mixtures
- 18 Comparison of Experimental Detonation Velocity,  $U_D$ , as a Function of the Log of the Initial Pressure,  $P_1$ , at Various Initial Temperatures,  $T_1$ , with the Results of Other Investigators for Stoichiometric ( $X_{H_2} = .667$ )  $H_2 - O_2$  Mixtures
- 19 Log of the Detonation Pressure Ratio,  $P_2/P_1$ , (obtained from experimental detonation velocity measurements) as a Function of the Initial Temperature,  $T_1$ , for Stoichiometric ( $X_{H_2} = .667$ )  $H_2 - O_2$  Mixtures
- 20 Photograph of the Test Setup for Detonation through Heterogeneous, Liquid-Gas Media
- 21 Schlieren Photographs of the Shattering of  $H_2O$  Droplets Behind  $H_2 - O_2$  Detonation Waves ( $X_{H_2} \approx .67$ )
- 22 Exploded View of Circular Test Section with Provision for Two-Dimensional Pressure Relief in Radial-Inward Direction
- 23 Schematic View of the Circular Test Section with Provision for Two-Dimensional Pressure Relief in Radial-Inward Direction
- 24 Schlieren Photographs of Stoichiometric, Hydrogen-Oxygen Detonation Waves in the Circular Test Section

## NOMENCLATURE - PART I

$a$ (ft/sec)	local speed of sound
$A_c$ (ft <sup>2</sup> )	chamber cross sectional area, $\ell_c x_n$
B	area ratio parameter, $\left(\frac{2}{\gamma + 1}\right)^{\frac{\gamma + 1}{2(\gamma - 1)}} \frac{\ell_t L}{A_c}$
$b, c$	constants introduced in the solution of the jump conditions
$C_p$ $\left(\frac{\text{ft-lb}}{\text{slug} \cdot ^\circ\text{R}}\right)$	specific heat at constant pressure
G	mass flow parameter, $\dot{m}_p / \rho_o v_o A_c N$
$\ell_t$ (ft)	width of the nozzle throat
L (ft)	distance between detonation waves, $2\pi R/N$
$\dot{m}$ $\left(\frac{\text{slugs}}{\text{sec}}\right)$	mass flow rate
$\bar{m}$	dimensionless mass flow rate, $\bar{\rho}\bar{v}$
$\dot{m}_p$ $\left(\frac{\text{slugs}}{\text{sec}}\right)$	total propellant mass flow rate
M	Mach number, $v/a$
N	number of waves in the engine
P (lb/ft <sup>2</sup> )	absolute pressure
Q $\left(\frac{\text{ft-lb}}{\text{slug}}\right)$	heat added per unit mass of unburned propellant
$\bar{Q}$	heat addition parameter, $Q/C_p T_o$
R (ft)	radius of curvature of the chamber centerline
T ( <sup>o</sup> R)	absolute temperature
$v$ (ft/sec)	circumferential velocity component
V (ft/sec)	magnitude of the velocity
$V_w$ (ft/sec)	absolute detonation wave velocity
$x, y$ (ft)	axial and circumferential coordinates
$\gamma$	ratio of specific heats
$\eta$	dimensionless circumferential coordinate, $y/L$

## NOMENCLATURE - PART I (continued)

$\xi$	dimensionless axial coordinate, $x/x_n$
$\mu$	relative mass concentration of the unburned propellant
$\rho \left( \frac{\text{slugs}}{\text{ft}^3} \right)$	mass density

### Subscripts

o	refers to condition at $y = 0$
1	refers to condition at $y = L$
a	refers to absolute velocity
A	refers to the unburned propellant
B	refers to the burned propellant
n	refers to condition at beginning of nozzle
p	refers to the initial propellant condition
t	refers to condition at nozzle throat
w	refers to the detonation wave
$\bar{f}$	denotes $f/f_0$

Note: Absence of subscript refers to the local condition in the chamber for the wave fixed system of coordinates.



## FOREWORD

This report is the Third Quarterly Progress Report, 1 December 1962 to 28 February 1963, on Contract No. AF 04(611)-8503, a contract between Edwards Air Force Base and The University of Michigan. The aim of this contract is to investigate the feasibility of a rotating detonation wave rocket motor.

Personnel associated with the various phases of the program as they are divided in the report are as follows:

I - G. Olsson, T. C. Adamson

II-A-G. L. Cosens, J. Brown

B-G. L. Cosens, K. Ragland

C-G. L. Cosens, F. Cheslak, S. Schmidt

D-E. Kurath

This project is directed by Professors J. A. Nicholls and R. E. Cullen of The University of Michigan. The Air Force Project Engineer is Richard Weiss (DGRR), 6593d Test Group (Development), Edwards Air Force Base, California.

## SUMMARY

This report presents the work accomplished on the rotating detonation wave engine feasibility program during the period 1 December 1962 to 28 February 1963.

The work described in this report represents a continuation of the supporting experimental and theoretical studies intended to consume approximately the first half of the program. The last half of the program will emphasize the design, fabrication and testing of a nominal 1000 lb-thrust, rocket motor utilizing the detonative mode of combustion and employing liquid oxygen and gaseous hydrogen as the propellants.

The theoretical studies concerning the behavior of detonation waves in heterogeneous liquid-gas media, and the heat transfer mechanism to the wall of a rotating detonation wave engine have been discontinued.

The theoretical study of an analytical model for the internal gas dynamics associated with a rotating detonation wave engine has been continued. The differential equations resulting from this analysis have been put in a form convenient for solution. Two cases of physical significance have been identified; the case of instantaneous, complete mixing between the burned and unburned propellants and the case of no mixing. An analytical solution to the equations has been found for the case where the local chamber pressure is equal or greater than the injector pressure and the injector mass flow is zero (blocked injector case). For the complete mixing case a digital computer program has been developed for the IBM 7090 computer which integrates numerically the differential equations. A solution has been obtained for the particular case where  $G = 1.0$ ,  $\gamma = 1.25$ ,  $\bar{T}_p = 0.0743$  resulting in the values of  $B = 2.36$ ,  $\bar{V}_w = 1.55$  and  $\bar{Q} = 0.741$  which satisfy both initial and final conditions of the differential equations and the hydrodynamic jump conditions across the detonation wave. Curves showing the behavior of the significant gas dynamic properties of the flow in the chamber for the complete mixing case as a function of the dimensionless circumferential coordinate,  $\eta$ , are presented. Also included on the plots for comparison is the case of the blocked injector. In addition, similarity and sizing relations for the internal gas dynamics of rotating detonation wave engines are presented.

The experimental studies on all of the phases reported in the first two Quarters have been continued.

- (1) The undesirable oscillatory nature of the output signal of the Kistler type 601 and 603 pressure transducers has been identified and suppressed. A "Fastax" camera has been utilized to identify the reason for malfunction in the starting sequence of the gaseous 100-lb thrust motor. It is concluded that initially two detonation waves are formed that move in opposite directions around the annular combustion chamber. All attempts made to eliminate this phenomena have proved unsuccessful up to this time.

- (2) The experimental determination of the effect of initial temperature and pressure on the detonation velocity is essentially complete. Extensive curves with comparison to data of other investigators is presented. It is concluded that the theoretical predictions of Reference 4, while agreeing in general with the experimental results of this investigation, tend to underestimate both the initial temperature and pressure effects on detonation velocities.
- (3) The experimental setup and procedure for investigating detonations in heterogeneous, liquid-gas media is described. A series of photographs is presented of  $H_2 - O_2$  detonation waves passing through a row of water droplets, 1mm in diameter. Indications are that the droplets are severely deformed and break into smaller droplets in the time interval of some 5 to 10  $\mu$ -sec after the passage of the wave. It is emphasized that the experiments are of preliminary nature.
- (4) A test section is described that provides for both the effects of curvature and two-dimensional pressure relief in the radial-inward direction. Schlieren photographs are presented that show the effects of relief on the detonation wave structure. Preliminary results indicate that the velocity of stoichiometric detonation waves is not affected by the combination of curvature and relief provided in the test section utilized.

# I. ANALYTICAL MODEL OF THE ROTATING DETONATION WAVE ENGINE

## A. INTRODUCTION

In Reference 1 the detailed development of a simplified analytical model of the rotating detonation wave engine was presented. Two special cases were considered:

- (1) complete instantaneous mixing between the burned and unburned propellants
- (2) no mixing between the burned and unburned propellants

In each case it has been found convenient to introduce the Mach number as a dependent variable and to put the differential equations in logarithmic differential form. Solutions to the equations are obtained by numerically integrating the differential equations and by utilizing the hydrodynamic jump conditions across the detonation wave to evaluate certain undetermined parameters.

It should be noted that the model of the flow in the engine between successive detonation waves is essentially a special case of the generalized (steady) one-dimensional flows discussed by Shapiro<sup>2</sup>. The procedure for putting the differential equations in a form convenient for solution is also adopted from Shapiro.

The similarity conditions for engine scaling are obtained by examining the dimensionless parameters which arise in the derivation of the non-dimensional form of the equations. The results are applied to develop sizing relations for engine design.

## B. THE COMPLETE MIXING CASE

On page 21 of Reference 1 the differential equations for the complete mixing case were expressed in the form

$$\left(\frac{\bar{P}\bar{v}}{\bar{a}^2}\right) \frac{d\mu}{d\eta} = (1 - \mu) G$$
$$\left(\frac{\bar{v}}{\bar{a}^2}\right) \frac{d\bar{P}}{d\eta} + \left(\frac{\bar{P}}{\bar{a}^2}\right) \frac{d\bar{v}}{d\eta} - \left(\frac{2\bar{P}\bar{v}}{\bar{a}^3}\right) \frac{d\bar{a}}{d\eta} = G - \frac{B\bar{P}}{M_o \bar{a}}$$

$$\left(\frac{1}{\gamma M_o^2}\right) \frac{d\bar{P}}{d\eta} + \left(\frac{\bar{P}\bar{v}}{\bar{a}^2}\right) \frac{d\bar{v}}{d\eta} = G(\bar{V}_w - \bar{v})$$

$$\left(\frac{(\gamma - 1) M_o^2 \bar{P}\bar{v}^2}{\bar{a}^2}\right) \frac{d\bar{v}}{d\eta} + \left(\frac{2\bar{P}\bar{v}}{\bar{a}}\right) \frac{d\bar{a}}{d\eta} = G \left[ \bar{T}_P + \frac{\gamma - 1}{2} M_o^2 \bar{V}_w^2 - \bar{a}^2 - \frac{\gamma - 1}{2} M_o^2 \bar{v}^2 \right]$$

The initial values of the dependent variables are

$$\bar{P}_o = \bar{v}_o = \bar{a}_o = 1, \quad \mu_o = 0 \quad \text{at } \eta = 0$$

and the hydrodynamic jump conditions across the detonation wave give the relations,

$$\begin{aligned} \bar{v}_1 &= b + \sqrt{b^2 + c} \\ \bar{P}_1 &= 1 - \gamma M_o^2 (\bar{v}_1 - 1) \\ \bar{a}_1 &= \sqrt{\bar{v}_1 [1 - \gamma M_o^2 (\bar{v}_1 - 1)]} \end{aligned}$$

with the constants b and c defined by

$$\begin{aligned} b &= \frac{1 + \gamma M_o^2}{(\gamma + 1) M_o^2} \\ c &= \frac{2}{(\gamma + 1) M_o^2} \left[ \mu_1 \bar{Q} - \frac{\gamma - 1}{2} M_o^2 - 1 \right] \end{aligned}$$

It is convenient to introduce the following notation:

$$\begin{aligned} M &= \frac{v}{a} = M_o \frac{\bar{v}}{\bar{a}} \\ \dot{\bar{m}} &= \bar{\rho}\bar{v} = \frac{\bar{P}\bar{v}}{\bar{a}^2} = \frac{\bar{P}M^2}{\bar{v}M_o^2} \\ d\dot{\bar{m}}_P &= \frac{\dot{m}_P dy}{\rho_o v_o A_c NL} = G d\eta \\ d\dot{\bar{m}}_n &= \frac{d\dot{m}_n}{\rho_o v_o A_c N} = \frac{B\bar{P}}{M_o \bar{a}} d\eta \end{aligned}$$

Note that

$$\frac{d\bar{m}_P}{\bar{m}} = \frac{\bar{v}M_o^2 G}{\bar{P}M^2} d\eta, \quad \frac{d\bar{m}_n}{\bar{m}} = \frac{B}{M} d\eta$$

$$\frac{dM}{M} = \frac{d\bar{v}}{\bar{v}} - \frac{d\bar{a}}{\bar{a}}$$

Then writing the equations in logarithmic differential form yields

$$\frac{d\mu}{1-\mu} = \frac{d\bar{m}_P}{\bar{m}}$$

$$\frac{d\bar{P}}{\bar{P}} + \frac{d\bar{v}}{\bar{v}} - 2 \frac{d\bar{a}}{\bar{a}} = \frac{d\bar{m}_P}{\bar{m}} - \frac{d\bar{m}_n}{\bar{m}}$$

$$\frac{1}{\gamma M^2} \frac{d\bar{P}}{\bar{P}} + \frac{d\bar{v}}{\bar{v}} = \left( \frac{\bar{V}_w - \bar{v}}{\bar{v}} \right) \frac{d\bar{m}_P}{\bar{m}}$$

$$(\gamma - 1) M^2 \frac{d\bar{v}}{\bar{v}} + 2 \frac{d\bar{a}}{\bar{a}} = \left[ \frac{M^2}{M_o^2 \bar{v}^2} \left( \bar{T}_P + \frac{\gamma - 1}{2} M_o^2 \bar{V}_w^2 \right) - \left( 1 + \frac{\gamma - 1}{2} M^2 \right) \right] \frac{d\bar{m}_P}{\bar{m}}$$

By applying Cramer's rule the differential quantities  $d\bar{P}/\bar{P}$ ,  $d\bar{v}/\bar{v}$ ,  $d\bar{a}/\bar{a}$  and hence  $dM/M$  can be found in terms of Mach number and the quantities on the right hand side of the equations. It is convenient to present the results in the form of a table of influence coefficients (see page 4).

As an example of the use of the table,  $d\bar{P}/\bar{P}$  is given by

$$\frac{d\bar{P}}{\bar{P}} = \frac{\gamma M^2}{M^2 - 1} \left\{ \left[ 1 - \frac{\bar{V}_w - \bar{v}}{\bar{v}} \left\{ 1 + (\gamma - 1) M^2 \right\} + \frac{M^2}{M_o^2 \bar{v}^2} \left( \bar{T}_P + \frac{\gamma - 1}{2} M_o^2 \bar{V}_w^2 \right) - \left( 1 + \frac{\gamma - 1}{2} M^2 \right) \right] \frac{\bar{v}M_o^2 G}{\bar{P}M^2} - \frac{B}{M} \right\} d\eta$$

	$\frac{d\bar{m}_P}{\bar{m}}$	$\frac{d\bar{m}_n}{\bar{m}}$	$\left(\frac{\bar{V}_w - \bar{v}}{\bar{v}}\right) \frac{d\bar{m}_P}{\bar{m}}$	$\left\{ \frac{M}{M_o^2 \bar{v}^2} \left[ \bar{T}_P + \frac{\gamma-1}{2} M_o^2 \bar{V}_w^2 \right] - \left[ 1 + \frac{\gamma-1}{2} M^2 \right] \right\} \frac{d\bar{m}_P}{\bar{m}}$
$\frac{d\bar{P}}{\bar{P}}$	$\frac{\gamma M^2}{M^2 - 1}$	$-\frac{\gamma M^2}{M^2 - 1}$	$-\frac{\gamma M^2 [1 + (\gamma - 1) M^2]}{M^2 - 1}$	$\frac{\gamma M^2}{M^2 - 1}$
$\frac{d\bar{v}}{\bar{v}}$	$-\frac{1}{M^2 - 1}$	$\frac{1}{M^2 - 1}$	$\frac{\gamma M^2}{M^2 - 1}$	$-\frac{1}{M^2 - 1}$
$\frac{d\bar{a}}{\bar{a}}$	$\frac{\frac{\gamma-1}{2} M^2}{M^2 - 1}$	$-\frac{\frac{\gamma-1}{2} M^2}{M^2 - 1}$	$-\frac{\frac{\gamma(\gamma-1)}{2} M^4}{M^2 - 1}$	$\frac{\frac{1}{2} (\gamma M^2 - 1)}{M^2 - 1}$
$\frac{dM}{M}$	$-\frac{1 + \frac{\gamma-1}{2} M^2}{M^2 - 1}$	$\frac{1 + \frac{\gamma-1}{2} M^2}{M^2 - 1}$	$\frac{\gamma M^2 \left(1 + \frac{\gamma-1}{2} M^2\right)}{M^2 - 1}$	$-\frac{\frac{1}{2} (1 + \gamma M^2)}{M^2 - 1}$
$\frac{d\mu}{1 - \mu}$	1	0	0	0

Evaluation of the Mach Number,  $M_o$ , of the Flow Just Behind the Detonation Wave

The derivative of the pressure at  $\eta = 0$  is

$$\left(\frac{d\bar{P}}{d\eta}\right)_{\eta=0} = \frac{\gamma M_o^2}{M_o^2 - 1} \left\{ \left[ \frac{\gamma-1}{2} M_o^2 (\bar{V}_w - 1)^2 - (\bar{V}_w - 1) + \bar{T}_P \right] G - \frac{B}{M_o} \right\}$$

From experimental evidence and physical reasoning one obtains the restriction

$$\left(\frac{d\bar{P}}{d\eta}\right)_{\eta=0} \leq 0$$

The quantity in braces,  $\left\{ \right\}$ , is a steadily increasing function of  $M_o$ . Consideration of the limiting values of the various terms results in

$$\begin{aligned} \frac{\gamma - 1}{2} &= O(.1), & B/G &= O(1) \\ \bar{V}_w - 1 &= O(1), & \bar{T}_P &= O(.1) \end{aligned}$$

and hence  $\left\{ \right\} \leq 0$  for a range of values of  $M_o$  including the interval  $0 \leq M_o \leq M_{o_c}$ , where  $M_{o_c}$  is the lowest positive root of the equation  $\left\{ \right\} = 0$ . By substituting the limiting values of the parameters into this equation it is found that  $M_{o_c} = O(10)$ . Therefore, because of the restriction on  $(d\bar{P}/d\eta)_{\eta=0}$ ,

$$\frac{\gamma M_o^2}{M_o^2 - 1} \geq 0$$

when  $0 \leq M_o < O(10)$ . In terms of  $M_o$  the condition becomes

$$M_o \geq 1$$

It should be noted that this restriction holds as long as  $M_o > 1$ . However, the detonation wave is considered to consist of a shock wave followed closely by a chemical reaction resulting in the release of energy in the form of heat. For this type of wave (see for example Reference 3 for a discussion of this matter)

$$M_o \leq 1$$

Comparison of the two restrictions on  $M_o$  shows that  $M_o = 1$  is the only possible case and hence that the detonation wave satisfies the Chapman-Jouguet condition. Note that this result implies  $(d\bar{P}/d\eta)_{\eta=0} \rightarrow -\infty$ .

#### Integration of the Equations for the Special Case $d\bar{m}_P = 0$

In a practical detonation wave engine the propellant injection pressure might be somewhat lower than the peak chamber pressure,  $P_o$ , behind the detonation wave and  $d\bar{m}_P$  would be zero until the local chamber pressure drops below the propellant injection pressure. Note that this analysis gives no consideration to the detailed dynamics of the flow of propellant through the injector orifices.



From the table of influence coefficients, the differential equation for the Mach number is, with  $d\bar{m}_P = 0$ ,

$$\frac{M^2 - 1}{1 + \frac{\gamma - 1}{2} M^2} dM = B d\eta$$

The initial condition is  $M = 1$  at  $\eta = 0$ . Hence integration results in

$$\frac{2}{\gamma - 1} (M - 1) - \frac{\gamma + 1}{\gamma - 1} \sqrt{\frac{2}{\gamma - 1}} \arctan\left(\frac{\sqrt{\frac{\gamma - 1}{2}} (M - 1)}{1 + \frac{\gamma - 1}{2} M}\right) = B\eta$$

In terms of the Mach number the pressure and velocity are given by

$$\bar{P} = \left[ \frac{\frac{\gamma + 1}{2}}{1 + \frac{\gamma - 1}{2} M^2} \right]^{\frac{2}{\gamma - 1}}$$

$$\bar{v} = M \sqrt{\frac{\frac{\gamma + 1}{2}}{1 + \frac{\gamma - 1}{2} M^2}}$$

Figure 1(a) displays the Mach number,  $M$ , as a function of  $B\eta$  for several values of the specific heat ratio,  $\gamma$ . Note the vertical tangent at  $\eta = 0$ . The dimensionless velocity and pressure as functions of  $B\eta$  are given in Figures 1(b) and 1(c). For a given value of the geometric parameter,  $B$ , the Mach number, velocity and pressure as functions of  $\eta$  can be found from Figure 1.

#### Results of the Numerical Integration of the Simultaneous Differential Equations for $M$ , $\bar{v}$ , $\bar{P}$ , and $\mu$

A digital routine for the IBM 7090 computer has been programmed which numerically integrates the simultaneous differential equations by the Runge-Kutta fourth-order method. This digital computer program has been utilized to solve the particular case  $G = 1.0$ ,  $\gamma = 1.25$ , and  $\bar{T}_P = 0.0743$ . The resulting values of  $B$ ,  $\bar{V}_w$ , and  $\bar{Q}$  which satisfy the jump conditions are

$$B = 2.36, \quad \bar{V}_w = 1.55, \quad \bar{Q} = 0.741$$

Figures 2(a) and 2(b) show the variation of  $M$ ,  $\bar{v}$ ,  $\bar{T}$ ,  $\bar{\rho v}$ ,  $\bar{P}$ , and  $\mu$  with  $\eta$ . Also,  $M$ ,  $\bar{v}$ ,  $\bar{T}$ , and  $\bar{P}$  versus  $\eta$  corresponding to the solution of the blocked injector case ( $d\bar{m}_p = 0$ ) with  $B = 2.36$  appear on the figures for comparison purposes.

The following conclusions can be drawn from the numerical results:

- (1) The absolute velocity,  $v_{1a}$ , of the gas just ahead of the detonation wave, which is given by the relation  $v_{1a} = v_o [\bar{V}_w - \bar{v}_1]$  can be estimated, since  $v_o \sim 5 \times 10^3$  ft/sec and from the numerical solution  $\bar{V}_w = 1.55$ ,  $\bar{v}_1 = 1.66$ . Hence  $v_{1a} \sim -500$  ft/sec. The minus sign indicates that the velocity is directed into the wave. The predicted magnitude of this velocity seems physically reasonable.
- (2) The relative concentration,  $\mu_1$ , of unburned propellant just ahead of the detonation wave is predicted to be only 0.667. Therefore, one result of complete instantaneous mixing between the burned and unburned propellants is that one third of the unburned propellant does not pass through the detonation wave and hence its chemical energy is not utilized. It is hoped that actual engine operation will correspond more closely to the assumption of no mixing between the burned and unburned propellants because in this case (for  $G = 1$ ) all of the unburned propellant will pass through the wave.
- (3) Examination of the detonation wave Mach number,  $M_1$ , and the pressure and velocity ratios,  $\bar{P}_1$ ,  $\bar{v}_1$ , across the detonation wave indicates that the use of one value of the specific heat ratio over the entire flow yields, for instance, somewhat low values of  $M_1$ . Relating  $\gamma$  to the relative concentration of unburned propellants,  $\mu$ , might result in an improvement of the complete mixing case analysis. It would also allow a better comparison of results with solutions for the no mixing case.

### C. THE NO-MIXING CASE

In the case of no mixing between the burned and unburned propellant the equations governing the flow were found to be in Reference 1 (note that  $M_o \equiv M_{B_o}$ )

$$G\eta d\bar{v}_A + \frac{\xi}{\gamma_B M_o^2} d\bar{P} = G(\bar{V}_w - \bar{v}_A) d\eta$$

$$d[\bar{\rho}_B \bar{v}_B (1 - \xi)] = -\frac{B\bar{P}}{M_o \bar{a}_B} d\eta$$

with the integrated relations

$$\bar{\rho}_A \bar{v}_A \xi = G\eta$$

$$\frac{\gamma_B - 1}{\gamma_A - 1} \bar{a}_A^2 + \frac{\gamma_B - 1}{2} M_o^2 \bar{v}_A^2 = \bar{C}_{P_A} \bar{T}_A + \frac{\gamma_B - 1}{2} M_o^2 \bar{V}_w^2$$

$$\bar{v}_B = \sqrt{1 + \frac{2}{(\gamma_B - 1) M_o^2} \left( \frac{\gamma_B - 1}{1 - \bar{P} \gamma_B} \right)}$$

$$\bar{a}_B = \bar{P}^{\frac{\gamma_B - 1}{2\gamma_B}}$$

$$\bar{\rho}_B = \bar{P}^{\frac{1}{\gamma_B}}$$

The initial conditions at  $\eta = 0$  are

$$\bar{v}_{B_o} = \bar{a}_{B_o} = \bar{P}_o = 1$$

$$\bar{v}_{A_o} = \bar{V}_w, \quad \bar{a}_{A_o} = \sqrt{\frac{\gamma_A - 1}{\gamma_B - 1} \bar{C}_{P_A} \bar{T}_P}$$

and the hydrodynamic jump conditions across the detonation wave give the relations

$$\bar{v}_{A_1} = b + \sqrt{b^2 + c}$$

$$\bar{P}_1 = 1 - \gamma_B M_o^2 (\bar{v}_{A_1} - 1)$$

$$\bar{a}_{A_1} = \sqrt{\frac{\gamma_A}{\gamma_B} [1 - \gamma_B M_o^2 (\bar{v}_{A_1} - 1)] \bar{v}_{A_1}}$$

where in this case

$$b = \frac{\gamma_A}{\gamma_B} \left[ \frac{1 + \gamma_B M_o^2}{(\gamma_A + 1) M_o^2} \right]$$

$$c = \frac{2}{\gamma_B - 1} \left( \frac{\gamma_A - 1}{\gamma_A + 1} \right) \frac{1}{M_o^2} \left[ \bar{Q} - \frac{\gamma_B - 1}{2} M_o^2 - 1 \right]$$

Introducing the Mach numbers,  $M_A$  and  $M_B$  (noting that  $M_o = 1$  in this case by an argument similar to that for the complete mixing case)

$$M_A = \frac{v_A}{a_A} = \frac{\bar{v}_A}{\bar{a}_A}$$

$$M_B = \frac{v_B}{a_B} = \frac{\bar{v}_B}{\bar{a}_B}$$

results in the differential relations

$$\frac{d\bar{v}_A}{\bar{v}_A} = \frac{1}{1 + \frac{\gamma_A - 1}{2} M_A^2} \frac{dM_A}{M_A}$$

$$\frac{d\bar{a}_A}{\bar{a}_A} = - \frac{\frac{\gamma_A - 1}{2} M_A^2}{1 + \frac{\gamma_A - 1}{2} M_A^2} \frac{dM_A}{M_A}$$

$$\frac{d\bar{P}}{\bar{P}} = - \frac{\gamma_B M_B^2}{1 + \frac{\gamma_B - 1}{2} M_B^2} \frac{dM_B}{M_B}$$

$$\frac{d\bar{v}_B}{\bar{v}_B} = \frac{1}{1 + \frac{\gamma_B - 1}{2} M_B^2} \frac{dM_B}{M_B}$$

$$\frac{d\bar{a}_B}{\bar{a}_B} = - \frac{\frac{\gamma_B - 1}{2} M_B^2}{1 + \frac{\gamma_B - 1}{2} M_B^2} \frac{dM_B}{M_B}$$

$$\frac{d\xi}{\xi} = \frac{d\eta}{\eta} - \frac{1 + (\gamma_A - 1) M_A^2}{1 + \frac{\gamma_A - 1}{2} M_A^2} \frac{dM_A}{M_A} + \frac{\gamma_B M_B^2}{1 + \frac{\gamma_B - 1}{2} M_B^2} \frac{dM_B}{M_B}$$

The integrated relationships are

$$\bar{P} = \left[ \frac{\frac{\gamma_B + 1}{2}}{1 + \frac{\gamma_B - 1}{2} M_B^2} \right]^{\frac{\gamma_B}{\gamma_B - 1}}$$

$$\bar{v}_B = M_B \left[ \frac{\frac{\gamma_B + 1}{2}}{1 + \frac{\gamma_B - 1}{2} M_B^2} \right]^{\frac{1}{2}}$$

$$a_B = \left[ \frac{\frac{\gamma_B + 1}{2}}{1 + \frac{\gamma_B - 1}{2} M_B^2} \right]^{\frac{1}{2}}$$

$$\bar{v}_A = M_A \left[ \frac{\frac{\gamma_A - 1}{\gamma_B - 1} \bar{C}_{P_A} \bar{T}_P + \frac{\gamma_A - 1}{2} \bar{V}_w^2}{1 + \frac{\gamma_A - 1}{2} M_A^2} \right]^{\frac{1}{2}}$$

$$\bar{a}_A = \left[ \frac{\frac{\gamma_A - 1}{\gamma_B - 1} \bar{C}_{P_A} \bar{T}_P + \frac{\gamma_A - 1}{2} \bar{V}_w^2}{1 + \frac{\gamma_A - 1}{2} M_A^2} \right]^{\frac{1}{2}}$$

$$\xi = \frac{1}{M_A} \left[ \frac{\frac{\gamma_A - 1}{\gamma_B - 1} \bar{C}_{P_A} \bar{T}_P + \frac{\gamma_A - 1}{2} \bar{V}_w^2}{1 + \frac{\gamma_A - 1}{2} M_A^2} \right]^{\frac{1}{2}} \left[ \frac{1 + \frac{\gamma_B - 1}{2} M_B^2}{\frac{\gamma_B + 1}{2}} \right]^{\frac{\gamma_B}{\gamma_B - 1}} \frac{\gamma_B}{\gamma_A} G \eta$$

The differential equations become

$$\frac{\xi}{1 + \frac{\gamma_A - 1}{2} M_A^2} \frac{dM_A}{M_A} - \left( \frac{\gamma_B M_B^2}{\gamma_A M_A^2} \right) \frac{\xi}{1 + \frac{\gamma_B - 1}{2} M_B^2} \frac{dM_B}{M_B} = \left( \frac{\bar{V}_w - \bar{v}_A}{\bar{v}_A} \right) \frac{G}{\rho_A \bar{v}_A} d\eta$$

$$\frac{\xi [1 + (\gamma_A - 1) M_A^2]}{1 + \frac{\gamma_A - 1}{2} M_A^2} \frac{dM_A}{M_A} - \frac{M_B^2 - 1 + \xi [1 + (\gamma_B - 1) M_B^2]}{1 + \frac{\gamma_B - 1}{2} M_B^2} \frac{dM_B}{M_B} = \left[ \frac{G}{\rho_A \bar{v}_A} - \frac{B}{M_B} \right] d\eta$$

Solving these equations by Cramer's rule one obtains the two simultaneous first order non-linear differential equations

$$\frac{1}{1 + \frac{\gamma_A - 1}{2} M_A^2} \cdot \frac{dM_A}{M_A} = \frac{\frac{\gamma_B M_B^2}{\gamma_A M_A^2} \left[ \frac{G}{\bar{\rho}_A \bar{v}_A} - \frac{B}{M_B} \right] - \left( \frac{\bar{v}_w - \bar{v}_A}{\bar{v}_A} \right) \frac{G}{\bar{\rho}_A \bar{v}_A} \cdot \left[ 1 + (\gamma_B - 1) M_B^2 + \frac{M_B^2 - 1}{\xi} \right]}{\xi \left\{ \frac{\gamma_B M_B^2}{\gamma_A M_A^2} [1 + (\gamma_A - 1) M_A^2] - [1 + (\gamma_B - 1) M_B^2] \right\} - (M_B^2 - 1)} \cdot d\eta$$

$$\frac{1}{1 + \frac{\gamma_B - 1}{2} M_B^2} \cdot \frac{dM_B}{M_B} = \frac{\left[ \frac{G}{\bar{\rho}_A \bar{v}_A} - \frac{B}{M_B} \right] - \left( \frac{\bar{v}_w - \bar{v}_A}{\bar{v}_A} \right) \frac{G}{\bar{\rho}_A \bar{v}_A} \cdot [1 + (\gamma_A - 1) M_A^2]}{\xi \left\{ \frac{\gamma_B M_B^2}{\gamma_A M_A^2} [1 + (\gamma_A - 1) M_A^2] - [1 + (\gamma_B - 1) M_B^2] \right\} - (M_B^2 - 1)} \cdot d\eta$$

The solution to the problem for the no mixing case involves the numerical integration of these equations starting with the appropriate initial values and finding numerically the parameters  $B$ ,  $\bar{T}_p$  and  $\bar{Q}$  that satisfy the jump conditions across the detonation wave. A digital computer program that will accomplish this is in preparation.

#### D. SIMILARITY AND SIZING RULES FOR THE INTERNAL GAS DYNAMICS OF ROTATING DETONATION WAVE ENGINES

The conditions for the similarity of different engine configurations are for the non-dimensional formulations of the differential equations, boundary conditions, and other pertinent relations to be identical for each configuration. One engine may be said to be a scale model of another if this conditions holds. In the following the non-dimensional parameters that occur in the simplified flow model are identified and the similarity rules for the internal gas dynamics of rotating detonation wave engines are derived. It is shown that there are three independent similarity parameters for the complete mixing case and five independent similarity parameters for the no mixing case.

In the equations for the complete mixing case the following non-dimensional parameters appear:

$$B = \frac{\ell_t L}{A_c} \left( \frac{2}{\gamma + 1} \right)^{\frac{\gamma + 1}{2(\gamma - 1)}} = \text{area ratio parameter}$$

$$G = \frac{\dot{m}_P}{\rho_o v_o A_c N} = \text{mass flow parameter}$$

$$M_o = \frac{v_o}{a_o} = \text{Mach number behind the detonation wave}$$

$$\bar{Q} = \frac{Q}{C_P T_o} = \text{heat addition parameter}$$

$$\bar{T}_P = \frac{T_P}{T_o} = \text{dimensionless propellant injection temperature}$$

$$\bar{V}_w = \frac{V_w}{v_o} = \text{dimensionless absolute wave velocity}$$

$\gamma$  = specific heat ratio

The question arises of how many of these parameters are determined by the problem and which parameters may be arbitrarily specified. The following comments relate to this issue:



- (1) From Section B, above,  $M_o = 1$ .
- (2) The propellant properties  $\gamma$ ,  $C_p$ ,  $Q$ , and  $T_p$  may be independently specified by the arbitrary choice of a propellant and the state of the propellant.
- (3) The geometric quantities  $l_t$ ,  $L$ , and  $A_c$  may all be independently specified also, in addition to the propellant mass flow rate  $\dot{m}_p$  and the number of waves in the engine,  $N$ .
- (4) There are three unknown dimensional quantities to be determined by the problem:  $\rho_o$ ,  $v_o$ , and  $V_w$ . (Note that  $a_o = v_o$  and  $T_o = a_o^2 / [(\gamma - 1) C_p]$ .) However, the three hydrodynamic jump conditions provide for the determination of these three unknowns.
- (5) In the dimensionless form of the problem (4) above indicates that only two of the five parameters  $G$ ,  $B$ ,  $\bar{T}_p$ ,  $\bar{Q}$ , and  $\bar{V}_w$  may be independently specified. The other three are found by obtaining solutions to the differential equations consistent with the jump conditions across the detonation wave.
- (6) It remains to choose which parameters should be independent. From the viewpoint of design, selecting values of  $G$  in the neighborhood of unity is physically significant since in the no-mixing case  $G = 1$  corresponds to 100% utilization of the propellant. Also, since the possible variation in  $T_o$  is of the order of  $\pm 10\%$ \*, reasonable values of  $\bar{T}_p$  can be selected without difficulty. Hence a solution to the problem is obtained in the form

$$\begin{aligned}
 B &= B(G, \bar{T}_p, \gamma) \\
 \bar{V}_w &= \bar{V}_w(G, \bar{T}_p, \gamma) \\
 \bar{Q} &= \bar{Q}(G, \bar{T}_p, \gamma) \\
 M &= M(\eta; G, \bar{T}_p, \gamma) \\
 \bar{v} &= \bar{v}(\eta; G, \bar{T}_p, \gamma) \\
 \bar{P} &= \bar{P}(\eta; G, \bar{T}_p, \gamma)
 \end{aligned}$$

Because of the functional form derived for the unknowns of the problem it is evident that  $G$ ,  $\bar{T}_p$ , and  $\gamma$  are the similarity parameters for the internal gas dynamics of rotating detonation wave engines when complete mixing between the burned and unburned

---

\*See Reference 4 for the results of theoretical calculations of detonation properties for a stoichiometric mixture of gaseous hydrogen and oxygen.

propellants is assumed to take place. It should be noted that the choice of  $G$  and  $\bar{T}_P$  as independent parameters is made arbitrarily.  $B$  and  $\bar{Q}$ , for instance, could be chosen just as well. Then the solution would be of the form  $M = M(\eta; B, \bar{Q}, \gamma)$ , etc., and  $B$ ,  $\bar{Q}$ , and  $\gamma$  would be the similarity parameters.  $G$  and  $\bar{T}_P$  have been selected here because physically meaningful values for them are available.

The sizing rules are found by expressing the quantities relating to engine geometry in terms of  $G$ ,  $B$ ,  $\bar{Q}$ , the propellant properties  $\gamma$  and  $Q$ , and the pressure,  $P_o$ :

$$NA_c = \frac{\dot{m}_P}{\gamma GP_o} \sqrt{(\gamma - 1) \frac{Q}{\bar{Q}}}$$

$$\ell_t R = \frac{\dot{m}_P B}{2\pi \gamma GP_o} \cdot \sqrt{(\gamma - 1) \frac{Q}{\bar{Q}}} \cdot \left(\frac{\gamma + 1}{2}\right)^{\frac{\gamma + 1}{2(\gamma - 1)}}$$

When no mixing is assumed to occur between the burned and unburned propellants the non-dimensional parameters that occur in the equations are

$$B = \frac{\ell_t L}{A_c} \left(\frac{2}{\gamma_B + 1}\right)^{\frac{\gamma_B + 1}{2(\gamma_B - 1)}} = \text{area ratio parameter}$$

$$\bar{C}_{P_A} = \frac{C_{P_A}}{C_{P_B}} = \text{ratio of the specific heat at constant pressure for the unburned propellants to that for the burned propellants}$$

$$G = \frac{\dot{m}_P}{\rho_{B_o} v_{B_o} A_c N} = \text{mass flow parameter}$$

$$M_o = \frac{v_{B_o}}{a_{B_o}} = \text{Mach number behind the detonation wave}$$

$$\bar{Q} = \frac{Q}{C_{P_B} T_{B_o}} = \text{heat addition parameter}$$

$$\bar{T}_P = \frac{T_P}{T_{B_o}} = \text{dimensionless propellant injection temperature}$$

$$\bar{V}_w = \frac{V_w}{v_{B_0}} = \text{dimensionless absolute wave velocity}$$

$\gamma_A, \gamma_B$  = specific heat ratios of the unburned and burned propellants, respectively

By an analysis similar to that for the complete mixing case the solution can be expressed in the functional form

$$B = B(G, \bar{T}_P, \bar{C}_{P_A}, \gamma_A, \gamma_B)$$

$$\bar{V}_w = \bar{V}_w(G, \bar{T}_P, \bar{C}_{P_A}, \gamma_A, \gamma_B)$$

$$\bar{Q} = \bar{Q}(G, \bar{T}_P, \bar{C}_{P_A}, \gamma_A, \gamma_B)$$

$$M_A = M_A(\eta; G, \bar{T}_P, \bar{C}_{P_A}, \gamma_A, \gamma_B)$$

$$M_B = M_B(\eta; G, \bar{T}_P, \bar{C}_{P_A}, \gamma_A, \gamma_B)$$

$$\xi = \xi(\eta; G, \bar{T}_P, \bar{C}_{P_A}, \gamma_A, \gamma_B)$$

Hence in the no-mixing case the similarity parameters are  $G, \bar{T}_P, \bar{C}_{P_A}, \gamma_A,$  and  $\gamma_B$ . The sizing rules are

$$NA_c = \frac{\dot{m}_P}{\gamma_B GP_0} \sqrt{(\gamma_B - 1) \frac{Q}{\bar{Q}}},$$

$$\ell_{tR} = \frac{\dot{m}_P B}{2\pi\gamma_B GP_0} \sqrt{(\gamma_B - 1) \frac{Q}{\bar{Q}}} \left( \frac{\gamma_B + 1}{2} \right)^{\frac{\gamma_B + 1}{2(\gamma_B - 1)}}$$

## E. APPLICATION OF SIMILARITY AND THE SIZING RULES TO PRELIMINARY DESIGN

In the preceding section the similarity laws and sizing rules predicted by the simplified analytical model of the rotating detonation wave engine are described. The following is one possible procedure for using these relations in the preliminary design of rotating

detonation wave engines (the relations derived for the no-mixing case are used here):

- (1) Specify the propellant, giving the values of  $\gamma_A$ ,  $\gamma_B$ ,  $C_{PA}$ ,  $C_{PB}$ ,  $Q$ , and  $T_P$ . Then  $\bar{C}_{PA}$  may be calculated.
- (2) Select the desired value of  $G$  and estimate  $\bar{T}_P$ .
- (3) Find the values of  $B$ ,  $\bar{V}_w$ , and  $\bar{Q}$  that satisfy the equations for the given values of  $G$ ,  $\bar{T}_P$ ,  $\bar{C}_{PA}$ ,  $\gamma_A$ , and  $\gamma_B$ .
- (4) Specify the propellant mass flow rate  $\dot{m}_P$ , engine radius  $R$ , and the number of detonation waves,  $N$ , in the engine. Also specify the peak pressure  $P_o$ .
- (5) Calculate the chamber cross-sectional area,  $A_c$ , and the throat width  $l_t$  from the scaling laws:

$$A_c = \frac{\dot{m}_P}{\gamma_B G N P_o} \sqrt{\frac{(\gamma_B - 1) Q}{Q}}$$

$$l_t = \frac{N \cdot B \cdot A_c}{2\pi \cdot R} \left( \frac{\gamma_B + 1}{2} \right)^{\frac{\gamma_B + 1}{2(\gamma_B - 1)}}$$

This analysis is to be applied to the design of the 1000 pound thrust rotating detonation wave engine.

## F. RESULTS AND CONCLUSIONS

Progress on obtaining solutions to the equations resulting from the simplified analysis of the rotating detonation wave engine given in Reference 1 has consisted of the following: The differential equations have been put in a form convenient for solution and in the complete mixing case a digital computer program to numerically integrate the differential equations has been developed. This computer program has been used to solve the case  $G = 1.0$ ,  $\bar{T}_P = 0.0743$ , and  $\gamma = 1.25$ . An analytic solution to the equations has been found for the special condition  $\dot{m}_P = 0$ . This corresponds physically to blockage of the injector flow when the local chamber pressure is greater than the injector pressure. Examination of the non-dimensional parameters appearing in the analysis has led to the establishment of sizing and similarity laws for the

internal gas dynamics of rotating detonation wave engines. A method of application of the sizing rules to engine design is presented.

Future work will consist of continuing the development of a digital computer program to integrate numerically the equations for the no-mixing case and of applying the results of the theoretical calculations to the design of the 1000 pound thrust engine. Comparisons of theoretical predictions with experimental results will be made when the pertinent data becomes available.

## II. EXPERIMENTAL STUDIES

### A. THE GASEOUS 100-LB THRUST MOTOR

The operating characteristics of a Kistler pressure transducer were investigated by flush mounting the instrument in the wall of a constant area detonation tube. Subsequent tests indicated that an unmodified Kistler pressure transducer (type 601 or 603 will produce undesirable high frequency oscillations whenever it is used to measure a sharp pressure pulse, e. g., the pressure rise across a shock or detonation wave. These oscillations occur at a frequency nearly equal to the natural frequency of the pickup, as specified by the manufacturer (300<sup>o</sup>KC for the type 603, and 150<sup>o</sup>KC for the type 601). The amplitude of the initial oscillation is in the order of 100% or more of the expected vertical deflection immediately following the detonation wave. The unsatisfactory nature of a typical pressure trace produced by an unmodified pickup is graphically illustrated in Figure 3(a).

Another group of researchers at The University of Michigan has obtained useful data from unmodified Kistler transducers by determining the average value associated with the oscillations. This technique is unstaible for evaluating the chamber pressure fluctuation in the rotating detonation wave engine because of its time-consuming nature.

The magnitude of these undesirable oscillations can be suppressed by the addition of a 27000  $\Omega$  resistor in series with the input side of the Kistler Model 566M charge-amplifier. Addition of this series resistor nearly eliminated the undesirable oscillations produced by the transducer without serious degradation of the rise-time, see Figure 3(b). Horizontal sweep time and vertical sensitivity associated with Figure 3(b) are 20  $\mu$ -sec/cm and .5 volt/cm respectively. Results obtained from the modified pressure transducer agree quite closely with the theoretical pressure-time history for one-dimensional Chapman-Jouguet detonation waves originating near the closed end of a detonation tube.

Addition of a wave trap to the output of the charge amplifier will theoretically eliminate the low amplitude oscillations shown in Figure 3(b).

The wall temperature trace shown in Figure 4 was obtained from a Nanmac thermocouple flush mounted in a constant area detonation tube (similar to the Kistler pressure transducer installation). Horizontal sweep time and the vertical sensitivity associated with Figure 4 are 2 milli-seconds/cm and 200  $\mu$ -volts/cm respectively. Thus far no attempt has been made to verify the 10  $\mu$ -sec rise time advertized by the manufacturer. Also, the results shown in Figure 4 are valid only for a detonation fabricated from yellow brass.

The "Fastax" 8mm and 16mm cameras have been utilized in obtaining information on the starting characteristics of the 100-lb thrust motor. Although the photographs shown in Figure 5 are from different runs they serve to illustrate the starting phase of the gaseous motor. Figure 5(a) shows the detonation wave emerging from the

starting tube and beginning to propagate around the annular combustion chamber in one direction. Figure 5(b) shows that there are now two detonation waves propagating in opposite directions. As the detonation wave emerges from the end of the starting tube it apparently forms an outwardly propagating spherical detonation wave resulting in the situation shown in Figure 5(b). Figure 5(c) shows the two waves just prior to collision. The reflected shock waves resulting from the collision of these two detonation waves are not of sufficient strength to reinitiate the detonation process.

All attempts to eliminate the propagation of detonation waves in both directions during the starting phase of the 100-lb thrust motor have proven unsuccessful. However, many of the more promising but time consuming schemes remain untried.

## B. TEMPERATURE AND PRESSURE EFFECTS ON $H_2 - O_2$ DETONATION VELOCITIES

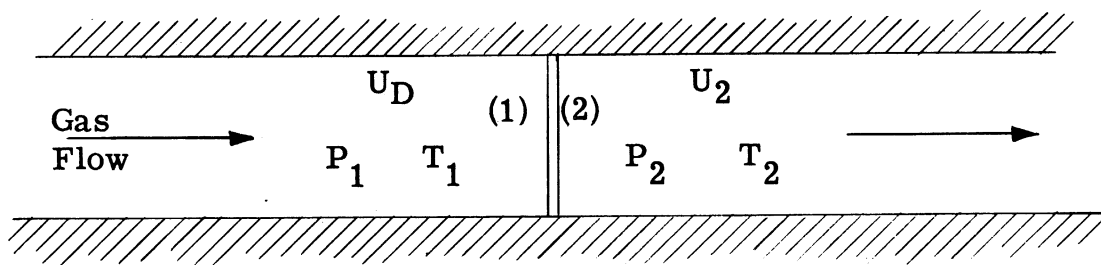
### 1. Introduction

The propellants of the rotating detonation wave engine can be injected into the combustion chamber in a gaseous state with temperatures near the oxygen vapor saturation point. However the detonation velocity of the hydrogen-oxygen propellants have never been determined at such low temperatures ( $110^\circ K$ ). Furthermore the velocity of detonation is a critical parameter in the design of the rotating detonation wave engine. Theoretical calculations of detonation velocity at these low temperatures and high pressures can conceivably be in error because of imperfect gas effects and lack of thermodynamic data. Experimentally, Moyle<sup>5</sup> obtained data on detonation velocities for hydrogen-oxygen mixtures at one atmosphere initial pressure and initial temperatures of  $160^\circ K$  to  $500^\circ K$ . Gealer<sup>6</sup> obtained data for room temperature  $H_2 - O_2$  mixtures over an initial pressure range of 1 to 68 atmospheres.

The purpose of this experiment is to obtain the detonation velocity of hydrogen-oxygen mixtures for use in the rotating detonation wave engine design over a range of initial temperatures from room temperature to the oxygen vapor saturation point ( $\sim 110^\circ K$ ) and initial pressures of 1 to 15 atmospheres. Stoichiometric and hydrogen-rich mixtures were considered of primary interest.

The design of this experiment has been greatly facilitated by Moyle<sup>5</sup> who showed that the detonation velocity for a mixture in a coiled tube is essentially the same as that for a straight tube (if the experiment is at ambient temperature and pressure).

The notation used throughout this section will be as shown below, utilizing a wave-fixed coordinate system with (1) representing the undisturbed gas and (2) the conditions behind the detonation wave. (at the Chapman-Jouguet plane, i. e. ,  $M_2 = 1$ ).



## 2. Test Equipment

A photograph of the test setup is shown in Figure 6 and a schematic of the test setup is presented in Figure 7. Mixing reservoirs were located in a blast proof pit outside the test room. The experiments were performed in a coiled tube shown in Figure 8. A straight tube was used to check the mixture ratio during the tests.

The velocity of the detonation wave was measured electronically by utilizing the ionized gases behind the detonation wave to trigger a time interval counter. This was accomplished by means of an ionization probe (Figure 9) as an input to a thyatron circuit. A schematic view of the velocity measurement system is shown in Figure 10.

The detonation coil was made of stainless steel tubing, 0.25" I. D. , 0.50" O. D. , 20 feet long and coiled in a 10 inch diameter. Three ionization probes were spaced 6 feet apart with 8 feet of coil before the first ionization probe. The straight detonation tube was also 0.25" I. D. stainless-steel tubing.

The hydrogen-oxygen mixtures were cooled to low temperatures in the following way: A double-walled stainless steel vessel was fabricated. This vessel was filled with a liquid with the lowest freezing point commercially available — isopentane (112°K). The isopentane was then cooled by bubbling liquid nitrogen through it, and then the detonation coil was immersed in the bath. Originally it was planned to obtain temperatures below 112°K by using liquid nitrogen under pressure as the liquid for the bath. This turned out not to be feasible because the detonation coil had to be removed from the bath after each run for reasons discussed later.

The temperature of the bath and the mixture were measured by four thermocouples in the bath and three thermocouples located in the detonation coil as shown in Figure 8.

A model airplane type glow plug was used to ignite the mixtures.

## 3. Methods and Procedures

The procedure for obtaining a single data point consisted of first bringing the detonation coil to room temperature, purging it with gaseous nitrogen, replacing the blow-out diaphragm and drawing a vacuum long enough to insure that the detonation coil was completely dry. Then the coil was immersed in the bath and allowed to come to the temperature of the bath. Finally the desired  $H_2 - O_2$  mixture was cooled to the bath temperature in a matter of seconds. Then the mixture was ignited.

This procedure had to be followed for each run; thus the test procedure was rather time consuming. It was found that the combustion products (water) froze on the walls of the detonation coil, and that unless the water was removed, erroneous results were obtained on the next run. Several methods were tried to eliminate the ice without removing the coil from the bath including a helium shock tube driver (gaseous piston), but due to the extremely rapid freezing process and the minute vapor pressure of ice at low temperatures these attempts were not successful.

A critical part of the experiment was the determination of the actual mixture ratio of  $H_2 - O_2$  used for a test. This was done by measuring the detonation velocity of a



given mixture at one atmosphere and 20°C in a straight detonation tube and comparing the result with the extensive data compiled by Moyle<sup>5</sup> and verified for stoichiometric mixtures in this experiment by partial pressure mixing; see Figure 11.

#### 4. Test Results

The results of the experiments are presented in Table 1. The results of detonation velocities for fully developed (Chapman-Jouguet) waves versus initial temperature of the mixture for initial pressures of 1, 5, 10, 15 atmospheres and 0.500, 0.667, 0.730 and 0.800 mole-fractions of hydrogen are plotted in Figures 12, 13, 14, and 15. The emphasis was placed on mixture ratios of 0.667 and 0.730 for motor design considerations. A cross-plot of detonation velocity versus mole-fraction of hydrogen is shown in Figure 16 for 10 atmospheres initial pressure. The data for stoichiometric mixtures was taken over an extended period of time and with mixtures slightly different than stoichiometric. This data was corrected as shown in Table 1 in order to base these runs on a true stoichiometric mixture. The data for mole-fractions of H<sub>2</sub> = 0.80 has a somewhat higher variation in mixture ratio ±0.01 because at one atmosphere initial pressure the mixture could not be detonated; therefore the extensive data of Moyle<sup>5</sup> at 1 atmosphere initial pressure could not be utilized to determine the more exact mixture ratio.

#### 5. Discussion of Test Results

The test results indicate that for a given initial pressure the detonation velocity increases at a slightly greater than linear rate as the initial temperature is lowered down to the saturation point of oxygen. The results for stoichiometric H<sub>2</sub> - O<sub>2</sub> mixtures are compared with the theoretical results of Zeleznik and Gordon<sup>4</sup>, and with the previous data of Gealer<sup>6</sup> and Moyle<sup>5</sup> in Figure 17.

In comparing theory with experiment it should be noted that the size of the detonation tube has a slight effect on the velocity. For one atmosphere and 20°C initial conditions Moyle<sup>5</sup> obtained the empirical equation  $U_D = U_\infty - \frac{22.8}{D}$  where D is the diameter of the detonation tube in inches,  $U_\infty$  is the detonation velocity in an infinite diameter tube and  $U_D$  is the detonation velocity in a tube of diameter = D. Thus for this experiment the 1 atmosphere, 20°C point should be raised about 90 ft/sec when comparing with theoretical results in order to correct for the tube-size effect. However it is expected that the tube size has a somewhat different though small effect as the density of the gas increases since this tube size effect is due to a combination of skin friction and heat transfer. The results indicate that the variation of initial conditions in both pressure and temperature have a somewhat greater effect on detonation velocity than predicted by theory.

In comparing theory with experiment it is useful to plot the detonation velocity versus the log of the initial pressure, as in Figure 18 for stoichiometric H<sub>2</sub> - O<sub>2</sub> mixtures. General agreement is obtained but experimentally the slope of the curve is slightly greater. Note the effect of tube size at one atmosphere and the increase in detonation velocity due to reduced initial temperature.

The predicted experimental pressure rise across a Chapman-Jouguet detonation wave may be calculated very simply once the detonation velocity is known by using the following well-known momentum relation developed from one-dimensional perfect-gas considerations:

$$\frac{P_2}{P_1} = \frac{1 + \frac{U_D^2 \bar{m}}{R_o T_1}}{1 + \gamma_2}$$

where  $\bar{m}$  is the average molecular weight of the undisturbed gas

$R_o$  is the universal gas constant

and  $\gamma_2$  is the ratio of specific heats behind the detonation wave (which from theory<sup>4</sup> is nearly constant)

The results of this calculation, shown in Figure 19 for stoichiometric  $H_2 - O_2$  mixtures indicate that a mixture initially at 10 atmospheres and 120°K will produce a peak pressure of 7,900 psia behind the wave.

### C. DETONATION THROUGH HETEROGENEOUS LIQUID-GAS MEDIA

In order that a rotating detonation wave engine will function properly, the fuel and the oxidizer must be in a form which will support a steady-state detonative process with the detonation wave presumably of the Chapman-Jouguet type. If part of the reactive mixture is present in the form of liquid droplets, any information regarding the effect of the two-phase (liquid-gas) nature of the initial reactants on the detonation process would be very important. A few considerations can be mentioned, e. g., injector design, wave (combustion) instability, and combustion efficiency. These considerations are of course of paramount importance to the proper operation of a conventional liquid-propellant rocket engine operating on the deflagrative-mode of combustion. It is believed that these considerations can be even of more importance to the proper design of a rocket engine operating on the detonative mode of combustion due to the extremely high reaction rates and short residence times associated with the detonative process.

It has been pointed out in the theoretical studies of References 1 and 7, that if the liquid droplets are large enough in size, it is quite probable that the detonative process could not be supported if the evaporation process is the only mechanism available to accelerate the change of phase, from liquid to gas, of the propellant involved. Another mechanism, the droplet shattering phenomenon was suggested as a possible means of accelerating this change of phase process. It is the purpose of this section to report on some preliminary experiments performed to shed some light on this phenomenon, or indeed to see if this phenomenon occurs at all in the time necessary to support a Chapman-Jouguet detonation wave.

The experimental study has been performed in the facility (see Figure 20) described as follows:

## Detonation Tube

This tube is built in sections, each section flanged and readily dismountable. The test section is fabricated of mild steel of 1" x 1" square inside cross section, 6 feet long, with a number of windows. A 4 foot detonation induction section is presently attached to it, and the tube is mounted horizontally. Extra sections can readily be added, and diaphragms inserted between sections. Thus, sections can be used for expansion chamber, detonation driver or constant volume combustor, or shock tube. It is at present set up as a detonation tube with glow plug ignition.

## Charging System

This system contains the plumbing, valves, etc., to charge the tube, premix the combustible mixtures, and purge the system after firing.

## Schlieren System for Optical Observation

This system utilizes 6-inch diameter, 54-inch focal length mirrors in a conventional single pass arrangement, auxiliary lenses to produce a magnified image (these are inside the shroud on the photograph of Figure 20), and a spark-discharge light source. The latter under favorable conditions will operate up to some 32 KV, with spark durations of about 0.1  $\mu$ -sec. The light source has an auxiliary lens mounted in front to increase the light intensity. The system is mounted on a bench and can be moved as desired to observe various locations in the test section.

## Electronics

This system consists of a thyratron sensing circuit and a time-interval counter for wave velocity measurements. In addition a time delay unit and power supply for the light source is required. These are actuated by ionization probes in the top wall of the test section. The first three pieces of equipment are also used on the experimental studies reported in Sections II-B and II-D of this report.

Operation of the detonation tube to date has been primarily concerned with determining the characteristics of the system and the potentialities of the schlieren optics. For this study hydrogen-oxygen detonations have been utilized because their properties are well known and they are convenient to handle. In this work some preliminary schlieren photographs of inert (water) droplets of approximately 1 mm diameter subject to detonation waves through stoichiometric  $H_2 - O_2$  mixtures have been obtained. These experiments will be discussed later. It appears that the present optical system and light source will be capable of magnifications up to approximately 5:1, and limited primarily by the light intensity and film speed and resolution. The photographs reproduced were taken with type 57 (3000 A. S. A.) polaroid film with less than full voltage on the light source, at a magnification of about 2.5:1. Larger magnifications are more demanding of adjustment and performance of the optics and timers. By utilizing a magnification of 5:1, with the optics in good focus and film resolution of 25 lines/mm, it would be possible to detect droplets down to a limit of about 8 microns in diameter. The present injector system can be used to form droplets in a limited size range (about 1mm) but of varying surface tension, viscosity, and density, and the liquid can be either inert or combustible in the environment in the tube. The drops can be subjected to a shock

wave rather than a detonation wave, and the Mach number of either wave can be varied by suitable choice of media. None of these permutations involve major changes in the system.

Earlier studies with a condensation chamber (Reference 1) indicated that a number of substances could be induced to form a mist of very fine droplets if introduced in the chamber as a gas and then quickly expanded. Unfortunately the materials tested all had very similar surface tensions. The droplets thus formed would be too small, i. e., a few microns diameter at most, to detect individually, but the gross characteristics of a detonation through a medium of this nature would be observable, e. g., detonation velocity, wave structure and stability. Droplets of intermediate size ( $10 \mu < D < 500 \mu$ ) will be more difficult to produce. This will require work on a suitable type of injector. Parameters other than diameter can be varied with no more difficulty than in the present setup, once the size range of droplets that a particular injector can produce, is known.

Included in this report is a sequence of spark-schlieren photographs (Figure 21) of a row of water droplets taken during the passage of several detonation waves. These photographs are not to be regarded as a finished product. There is a need of technical improvement, particularly in the focus. The system is still in the process of being explored and adjusted, and these photographs were obtained as a step in that process.

The observed detonations take place through approximately stoichiometric mixtures of hydrogen and oxygen with initial conditions atmospheric pressure and approximately room temperature. Wave initiation is obtained with a glow plug. Previous measurements indicate that detonations through such a mixture is fully developed and steady, i. e., a Chapman-Jouguet wave, within 5 1/2 feet of the point of ignition. Photographs are taken at a station about 9 feet from the glow plug end of the tube. The other end of the tube is closed with an aluminum foil diaphragm for each run. Detonation velocity is about 9800 ft/sec (mixture is slightly hydrogen-rich). Water droplets are introduced by an injector in the top of the tube, and fall vertically into a drain in the bottom of the tube. The injector is a Number 22 steel hypodermic needle held in a fitting and fed with approximately one inch Hg nitrogen pressure. Droplet velocity is small. A number of photographs of the droplet stream indicate the droplets average 1.0mm diameter, spaced 3/32 to 1/8 vertically, when the injector pressure is properly adjusted. Droplet diameter is fairly constant. Photograph (0) of Figure 21 is included of the undisturbed droplet stream. Photographs are on 4 x 5 Polaroid film (3000 A.S.A.). The spark light source was used at 75% to 80% of maximum voltage, due to humid atmospheric conditions, with condensing lens set for a 4:1 increase in light intensity. The knife edge setting was approximately 15% cutoff. Less cutoff will be used in future studies, since a less sensitive schlieren photograph will give a clearer indication of what is happening immediately in the vicinity of the drops. Magnification is 2.5:1. The wave proceeds from left to right on each photograph. Diagonal lines at the left of the photographs are reference wires attached to the outside of the tube. Each photograph is of a different set of droplets. In the succeeding photographs the waves are .6 inch (actual) to 1.7 inch downstream of the drops, which is equivalent to some 5 to 15 microseconds. Droplets in question are in a vertical row in each photograph. Any other

droplets appearing in the photographs originated from collections of water which was deposited on the wall when the injector was being adjusted before the run, and are to be disregarded. The starting technique has been improved subsequent to the photographs, to eliminate this effect.

It can be seen that the left edge of the droplets is at about the same location in each photograph, but that the apparent vertical diameter, and extension to the right, increase rapidly. The drops are severely deformed after 5 microseconds. In photograph (1), interconnecting shocks can be seen between the droplets. In subsequent photographs these have degenerated into strong pressure gradients.

It is to be noted that if the apparent droplet diameter triples, the apparent surface area will be increased by a factor of 9 and the volume by 27. Hence the droplets must be very tenuous in the later pictures of the sequence. Therefore, the amount of droplet surface area available for subsequent evaporation and combustion is far greater than in the undisturbed drop.

With reduced sensitivity in the schlieren photographs it might be possible to tell whether individual small droplets still exist or whether an appreciable part of the liquid is already changing phase.

It is to be emphasized that this set of data is of preliminary nature only. However, it does point to a number of avenues of inquiry that are of paramount interest in this study. In addition, it indicates that the present system is capable of producing acceptable results, once refinements and adjustments have been made. It also shows that the system is capable of yielding considerable information on droplet-detonation mechanisms without basic changes.

#### D. GEOMETRICAL TESTS

A test section has been fabricated for studying the effect of two-dimensional pressure relief behind a detonation wave. An exploded view of the section is shown on the picture of Figure 22. A schematic drawing of the section used is shown on Figure 23.

With each firing of the section, the velocity of the detonation wave is measured in the driver section in addition to a measurement of the time delay for the spark light source discharge, using two CMC Model 757-BN time-interval counters. The schlieren system, thyatron triggered, spark light source and glow plug ignition are described in Reference 1.

The frame used for holding film is shown on the photograph of Figure 22. A film on the frame separates the combustible pre-mixed gases in the test section from the inert air outside. A bowl (7 in. diameter x 3 in. deep) filled with distilled water is used for making the film of a 15% (by volume) collodion in amyl acetate solution. Two drops of this solution are first spread on the surface of the water. After this dries, leaving a film on the surface of the water, the frame held by a pair of hemostats is inserted under the film. By lifting the frame slowly, the film attaches to both sides. The frame is now inserted in the test section and the test section is assembled.

The film of double thickness used with the two drops of liquid is believed to be about 1000 Å thick.\* This is the thinnest film readily attainable. Many other methods of applying the film with various thicknesses were attempted but proved to be unsuccessful.

The assembled test section is now attached to a detonation tube driver section (described in Reference 1). Using a known mixture of H<sub>2</sub> - O<sub>2</sub> the pre-mixed gas is bled through the tube and curved section for about a 1 minute period. (This time is sufficiently long to assure purging and a uniform mixture in the section.) Then immediately after closing the charging valve, the end of the section is sealed with masking tape and a detonation wave is fired through the section.

If a schlieren system is used it has been observed that a complete blockage of the light through the windows can occur. It is believed that the knife-edge acts as a polarizing device and the curved glass windows as another since rotating the knife edge varies the intensity of light coming through the windows. Ordinary plate glass has been used. The same type of phenomena was experienced with plastic windows and was one of the reasons they were discarded in favor of glass. The other reason is that the plastic quickly develops a surface imperfection due to the highly convective gases behind the detonation wave.

A number of experimental runs have been made to date. Figures 24(a) and 24(b) are photographs of stoichiometric detonation waves propagating in a curved channel with 24(a) having pressure relief in the radial-inward direction, with 24(b) having a steel wall insert on the inside radius. Figure 24(a) compares favorably with similar test results made by Dabora of a detonation wave expanding two-dimensionally into air in a straight tube. The detonation wave appears to be unconfined. Figure 24(b) is similar to Figure 14 of Reference 1 in that it shows some of the reflected shock waves in the gases immediately behind the detonation wave.

Although results have not been completely analyzed yet, it appears that the effects of two-dimensional pressure relief in the radial-inward direction and curvature reach a steady state almost as soon as the detonation wave encounters the curved section. This is apparent when comparison of many runs of detonation waves in different positions in the section indicate constant profile. Some preliminary results (not shown) on the effect of two-dimensional pressure relief on the detonation wave velocity can be mentioned. Within the limits of experimental scatter utilizing nearly-stoichiometric H<sub>2</sub> - O<sub>2</sub> mixtures, it has been observed by plotting the position of different waves on a time-distance plot, that the detonation waves with two-dimensional relief propagate at the same velocities in the curved test section as do waves confined by a steel wall on the inner radius. This effect must be studied further and in particular tests using hydrogen-rich mixtures will be utilized.

---

\*Dabora, E. , (Unpublished work being performed at this laboratory).

It was found that the curved section shown in Figure 13 of Reference 1 was non-uniform in its cross section (i. e. , 1/2" x 3/8") so that a new section is being assembled with correction of this error. Some minor modifications in design are also being incorporated into this section. Glass windows instead of plexiglas have been cut and will be used.

### III. STUDY PLANS FOR NEXT QUARTER

The theoretical studies involving the simplified analytical model of the rotating detonation wave engine will be continued. Emphasis will be placed on the development of a digital computer program to integrate numerically the equations for the no-mixing case and the application of the results to the design of the 1000 lb-thrust engine. Comparison of the theoretical predictions with experimental results from the 100 lb-thrust motor will be critically examined to check on the validity of the analytical model.

The work involving the gaseous, 100 lb-thrust motor will be concerned initially with obtaining a solution to the starting problem. Following this, a study of the effects of certain critical parameters such as propellant mass flow, mixture ratio, injector geometry, axial chamber length, and nozzle throat size on the measurable properties, i. e., wave velocity, chamber pressure, wall temperature, etc., will be made.

Experiments concerning the effect of curvature and relief on detonation wave characteristics will be terminated when conclusive results on the effect of mixture-ratio are obtained.

Experiments will continue in an attempt to obtain critical design information at an early date concerning the droplet breakup mechanism behind strong shock waves.

Design will continue on the 1000 lb -thrust motor. In addition, the Willow Run Rocket Test Site will be made ready for the subsequent test program.



## REFERENCES

1. Nicholls, J. A. , and Cullen, R. E. , et al. , 'The Feasibility of a Rotating Detonation Wave Rocket Motor,' Univ. of Mich. Eng. Res. Inst. Report 05179-2-P, December 1962.
2. Shapiro, A. H. , The Dynamics and Thermodynamics of Compressible Fluid Flow, Vol. I, Chapter 8, The Ronald Press Co. , New York, 1953.
3. Courant, R. , and Friedrichs, K. O. , Supersonic Flow and Shock Waves, Chapter III, Part E, Interscience Publishers, Inc. , New York, 1948.
4. Zeleznick, F. J. , and Gordon, S. , "Calculation of Detonation Properties and Effect of Independent Parameters on Gaseous Detonations," ARS Journal, 32, 606 (1962).
5. Moyle, M. P. , "The Effect of Temperature on the Detonation Characteristics of Hydrogen-Oxygen Mixtures," Industry Program Report IP-195, The University of Michigan, December 1956.
6. Gealer, R. L. , "The Influence of High Pressure on the Properties of Hydrogen-Oxygen Detonation Waves," Industry Program Report IP-295, The University of Michigan, June 1958.
7. Nicholls, J. A. , and Cullen, R. E. , et al. , 'The Feasibility of a Rotating Detonation Wave Rocket Motor,' Univ. of Mich. Eng. Res. Inst. Report 05179-1-P, August 1962.

TABLE I

EXPERIMENTAL DETONATION VELOCITIES OF H<sub>2</sub> - O<sub>2</sub> MIXTURES  
AT REDUCED INITIAL TEMPERATURES AND INCREASED INITIAL PRESSURES

Tube I. D. = 1/4 in.

Coil I. D. = 1/4 in.

$$X_{H_2} = 0.500 \pm .005$$

Run No.	P <sub>1</sub> (atm)	T <sub>1</sub> (°K)	Time in Tube (μ-sec)	Time in Coil (μ-sec)	U <sub>D</sub> (ft/sec)
41	1	293	399		7519
42	1	293	398		7538
43	1	293	400		7500
45	1	113		778	7712
46	1	126		781	7682
47	1	134		785	7643
48	1	148		784	7653
50	1	178		792	7575
51	1	197		795	7547
52	1	293		806	7444
53	1	293		808	7425
54	1	293		807	7434
55	1	217		798	7518
56	1	228		799	7509

TABLE I (continued)

$$X_{H_2} = 0.667 \pm .0025$$

(Note: Corrected data based on 330  $\mu$ -seconds in straight tube (9090 ft/sec) as the correct time for  $X_{H_2} = 0.667$ .)

Run No.	P <sub>1</sub> (atm)	T <sub>1</sub> (°K)	Time in Tube ( $\mu$ -sec)	Time in Coil ( $\mu$ -sec)	U <sub>D</sub> (ft/sec)	Corrected Time ( $\mu$ -sec)	Corrected U <sub>D</sub> (ft/sec)
1	1	293	327		9174		
2	1	293	328		9146		
3	1	293	327		9147		
5	1	293		656	9146	662	9063
6	1	293		656	9146	662	9063
7	1	293		656	9146	662	9063
8	1	293		654	9176	660	9091
9	1	293	323		9288		
10	1	293	323		9288		
11	1	197		642	9345	656	9146
12	1	293	324		9259		
13	1	208		642	9345	654	9176
14	1	293	325		9231		
15	1	217		643	9331	653	9188
16	1	225		644	9316	654	9176
17	1	220		645	9302	655	9160
18	1	293	324		9259		
19	1	169		638	9404	650	9231
20	1	111		623	9630	635	9449
21	1	130		629	9538	641	9360
22	1	169		639	9389	651	9217
23	1	186		641	9360	653	9188
24	1	199		641	9360	653	9188
28	1	263		652	9202	664	9036
33	1	113		625	9600	637	9419
73	1	293	325		9231		
74	1	293	325		9231		
77	1	293	326		9202		
78	5	284		615	9756	625	9600
79	5	284		616	9740	626	9585

TABLE I (continued)

Run No.	P <sub>1</sub> (atm)	T <sub>1</sub> (°K)	Time in Tube (μ-sec)	Time in Coil (μ-sec)	U <sub>D</sub> (ft/sec)	Corrected Time (μ-sec)	Corrected U <sub>D</sub> (ft/sec)
83	5	251		613	9787	623	9631
84	5	116		597	10,050	607	9884
85	5	140		600	10,000	610	9834
86	5	155		605	9917	615	9756
87	5	165		605	9917	615	9756
88	5	115		596	10,066	606	9900
90	5	184		605	9917	615	9756
91	5	217		610	9834	620	9677
57	1	293	327		9174		
58	1	293	327		9174		
59	1	293	327		9174		
60	10	183		593	10,118	599	10,017
66	1	293	326		9202		
67	1	293	327		9174		
68	10	173		592	10,135	599	10,017
69	10	143		590	10,169	597	10,050
70	10	122		587	10,221	594	10,101
71	10	289		608	9868	615	9756
72	10	114		588	10,204	595	10,084
73	1	293	325		9230		
74	1	293	325		9230		
80	10	284		604	9933	614	9772
81	10	284		603	9950	613	9788
82	10	246		602	9966	612	9804
89	10	117		585	10,256	595	10,084
126	1	293	327		9174		
127	1	293	326		9202		
128	1	293	327		9174		
129	1	293	326		9202		
130	15	288		601	9983	608	9868
131	15	288		601	9983	608	9868
132	15	125		584	10,274	591	10,152
133	15	134		586	10,239	593	10,118
134	15	153		590	10,160	597	10,050
135	15	164		588	10,204	595	10,084
136	15	209		594	10,101	601	9983

TABLE I (continued)

$$X_{H_2} = 0.730 \pm .005$$

Run No.	P <sub>1</sub> (atm)	T <sub>1</sub> (°K)	Time in Tube (μ-sec)	Time in Coil (μ-sec)	U <sub>D</sub> (ft/sec)
25	1	293	301		9967
26	1	293	300		10,000
27	1	293	299		10,033
29	1	293		602	9966
30	1	293		604	9934
31	1	293		604	9934
32	1	293		604	9934
34	1	129		578	10,381
35	1	152		583	10,201
36	1	158		587	10,221
37	1	174		589	10,186
38	1	193		591	10,152
39	1	203		591	10,152
40	1	222		595	10,084
44	1	113		572	10,489
92	1	291	300		10,000
93	1	291	299		10,033
94	1	291	299		10,033
95	1	291	300		10,000
96	5	291		578	10,381
97	5	291		578	10,381
104	5	113		559	10,733
105	5	118		559	10,733
106	5	137		561	10,695
107	5	155		563	10,657
109	5	203		567	10,582
98	10	291		563	10,657
99	10	291		563	10,657
100	10	138		549	10,929
101	10	161		552	10,861
102	10	120		548	10,949
103	10	118		547	10,969
108	10	197		556	10,791

TABLE I (continued)

$$X_{H_2} = 0.80 \pm .01$$

Run No.	P <sub>1</sub> (atm)	T <sub>1</sub> (°K)	Time in Tube (μ-sec)	Time in Coil (μ-sec)	U <sub>D</sub> (ft/sec)
110	10	291	263	11,407	
111	10	291	264	11,364	
112	5	291	267	11,236	
113	5	291	267	11,236	
114	5	291	267	11,236	
115	10	291	263	11,407	
116	10	288		527	11,385
117	10	288		527	11,385
118	10	288		526	11,407
119	10	116		516	11,628
120	10	119		516	11,628
121	10	133		516	11,628
122	10	148		520	11,538
123	10	163		520	11,538
124	10	203		521	11,516

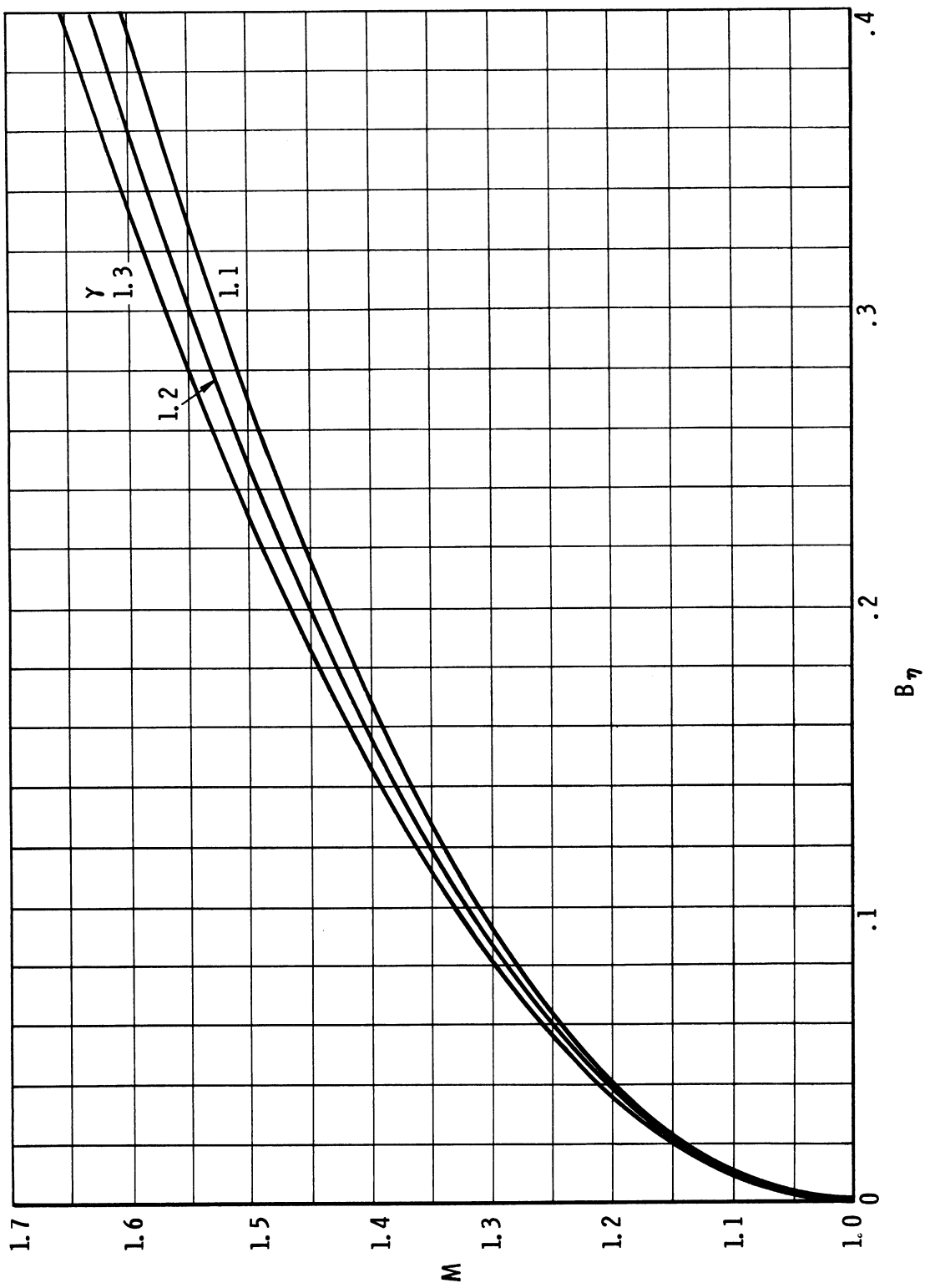


Figure 1(a). Mach Number,  $M$ , as a Function of the  $B_\eta$  Product for the Case of a Blocked Injector ( $\text{dim}_p = 0$ )

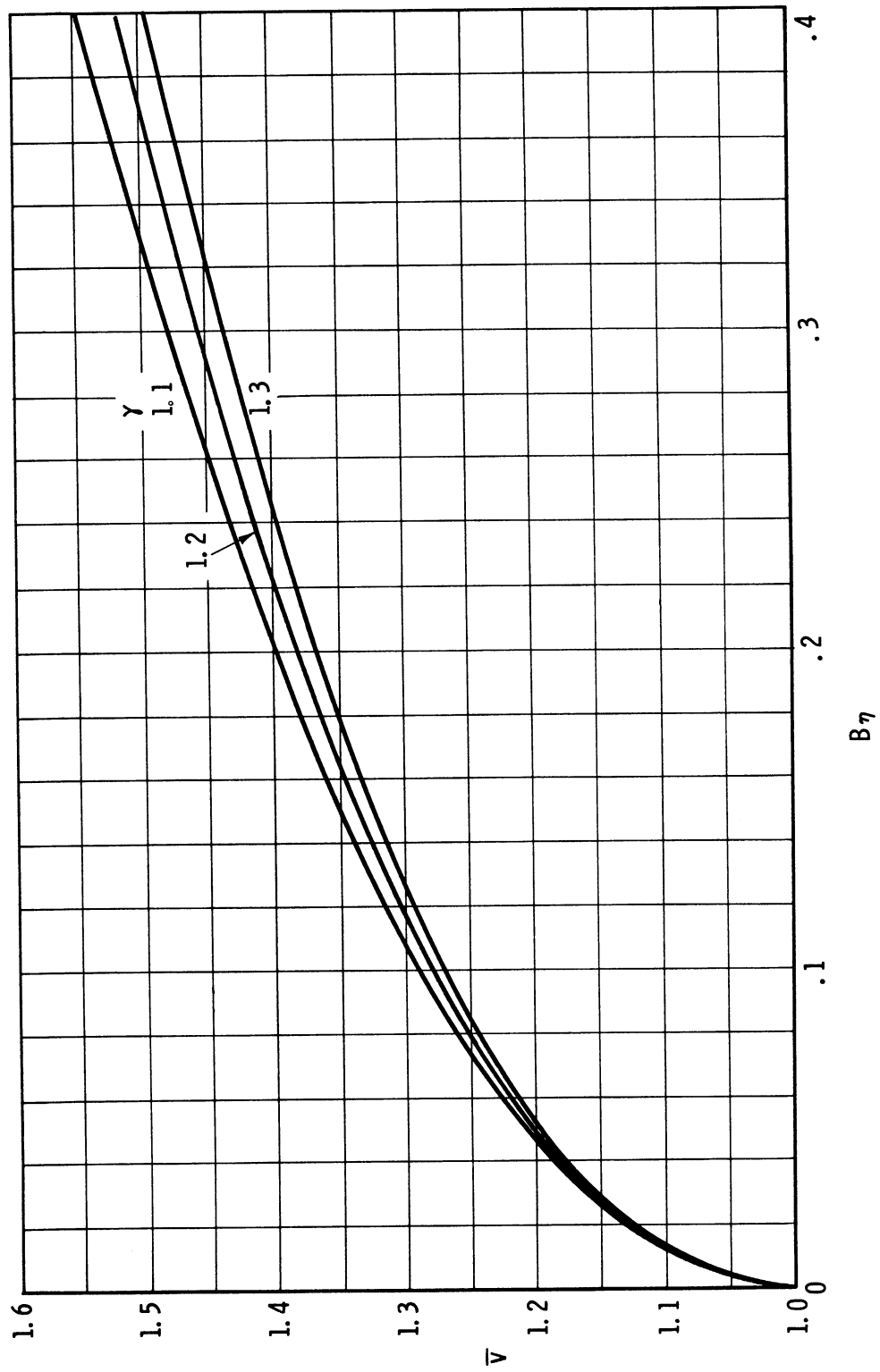


Figure 1(b). Dimensionless Velocity,  $\bar{v}$ , as a Function of the  $B\gamma$  Product for the Case of a Blocked Injector ( $dm_p = 0$ )



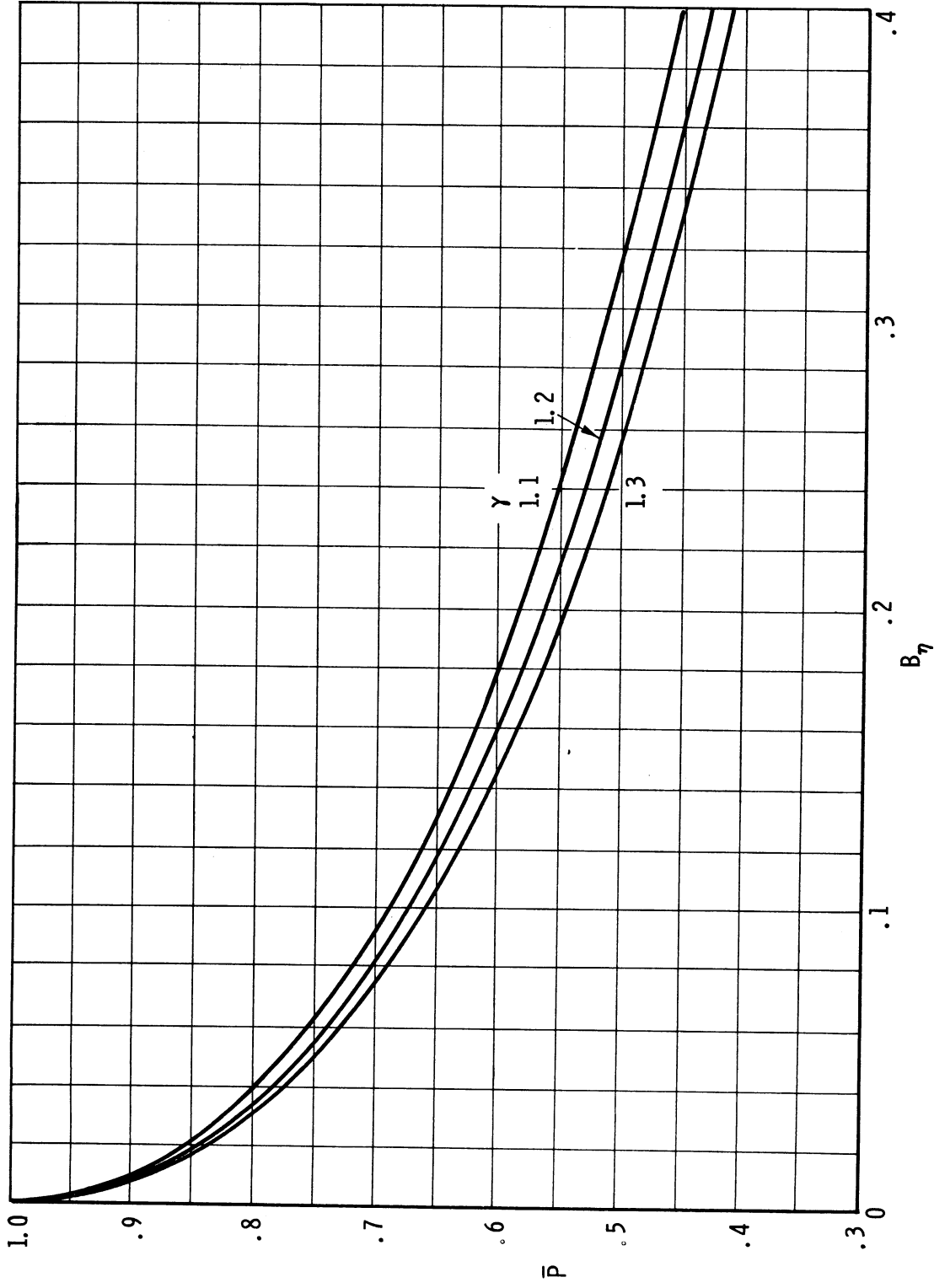


Figure 1(c). Dimensionless Pressure,  $\bar{P}$ , as a Function of the  $B_\eta$  Product for the Case of a Blocked Injector ( $dm_P = 0$ )

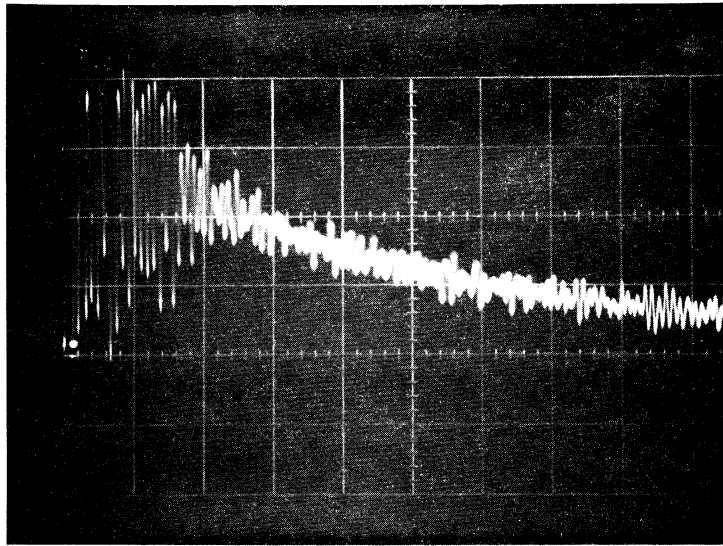


Figure 3(a). Pressure Profile of an  $H_2 - O_2$  Detonation Wave in a Straight Tube Using an Unmodified Kistler Pressure Transducer

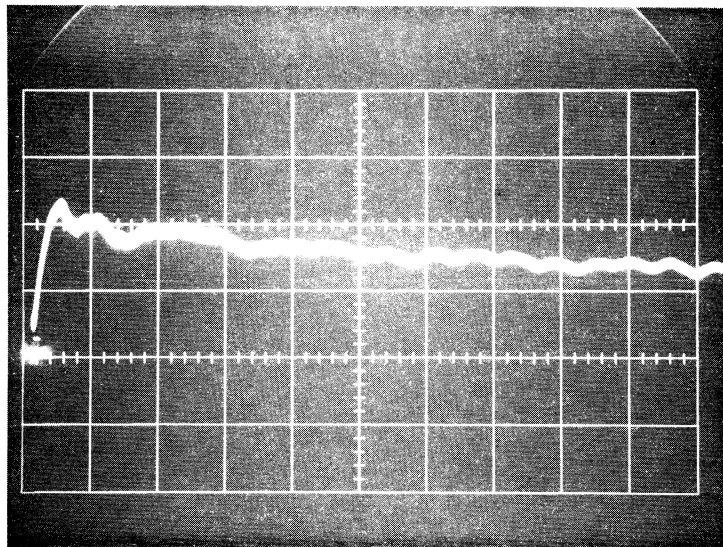


Figure 3(b). Pressure Profile of an  $H_2 - O_2$  Detonation Wave in a Straight Tube Using a Modified Kistler Pressure Transducer

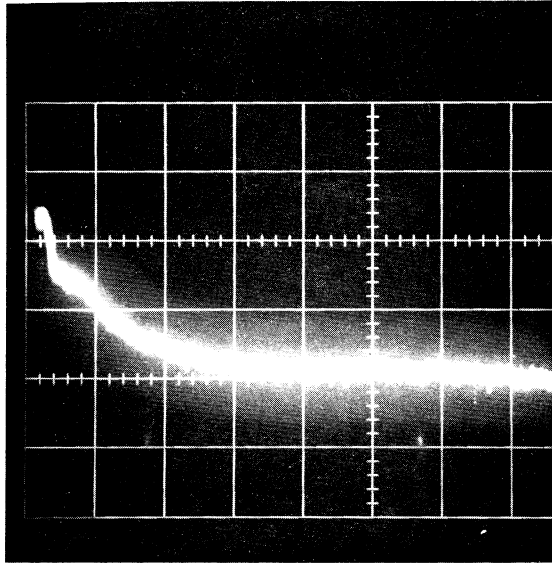


Figure 4. Wall Temperature Profile Behind an  $H_2 - O_2$  Detonation Wave in a Straight Tube Using a Nanmac Wall Thermocouple



a



b



c

Figure 5. Photographs of the Starting Sequence of the Gaseous, 100-lb Thrust Motor Obtained by a 'Fastax' 8mm Framing Camera

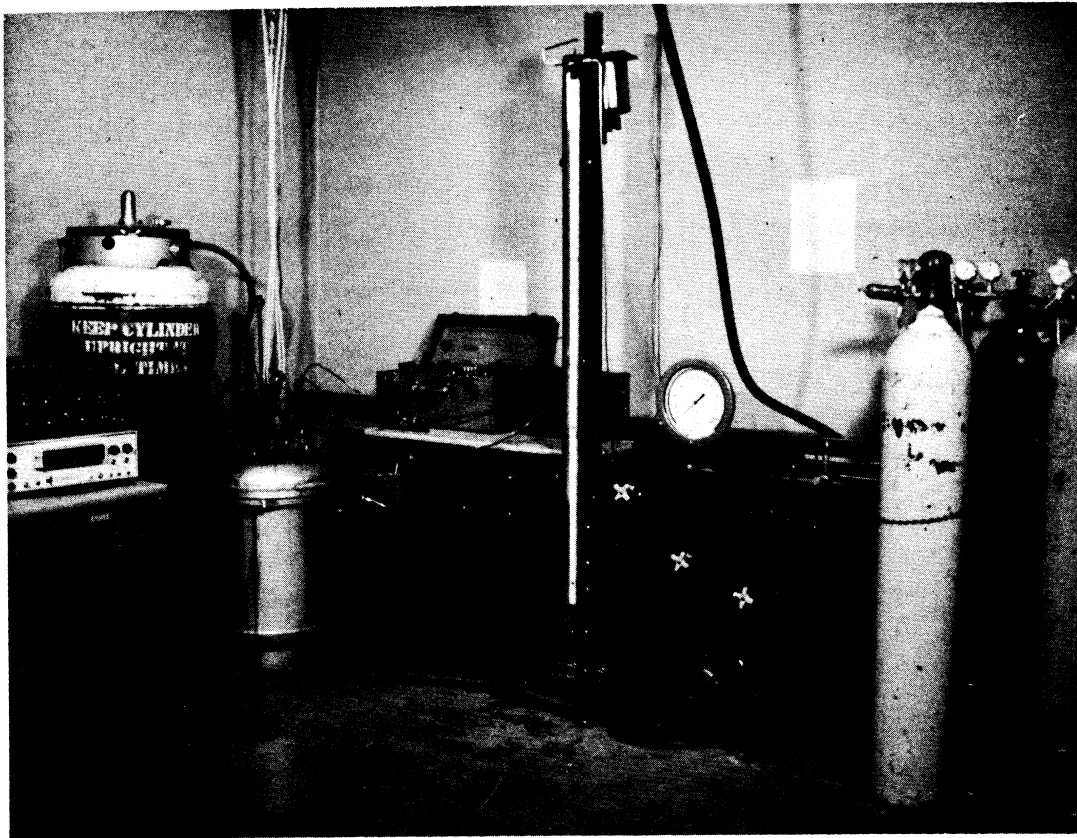


Figure 6. Photograph of the Test Setup for the Measurement of the Temperature and Pressure Effects on Hydrogen-Oxygen Detonation Velocities

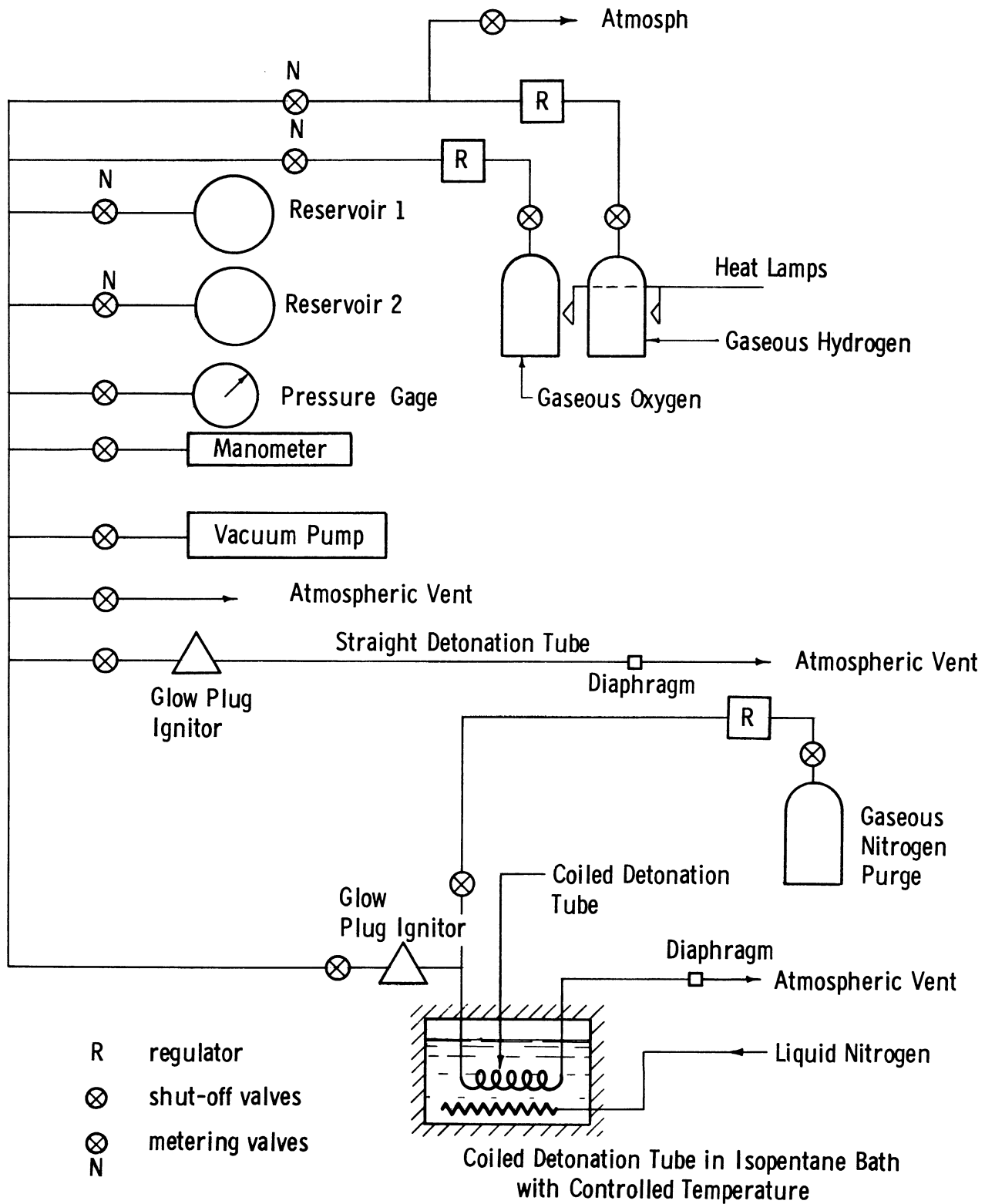


Figure 7. Schematic View of the Test Setup for the Measurement of the Temperature and Pressure Effects on Hydrogen-Oxygen Detonation Velocities

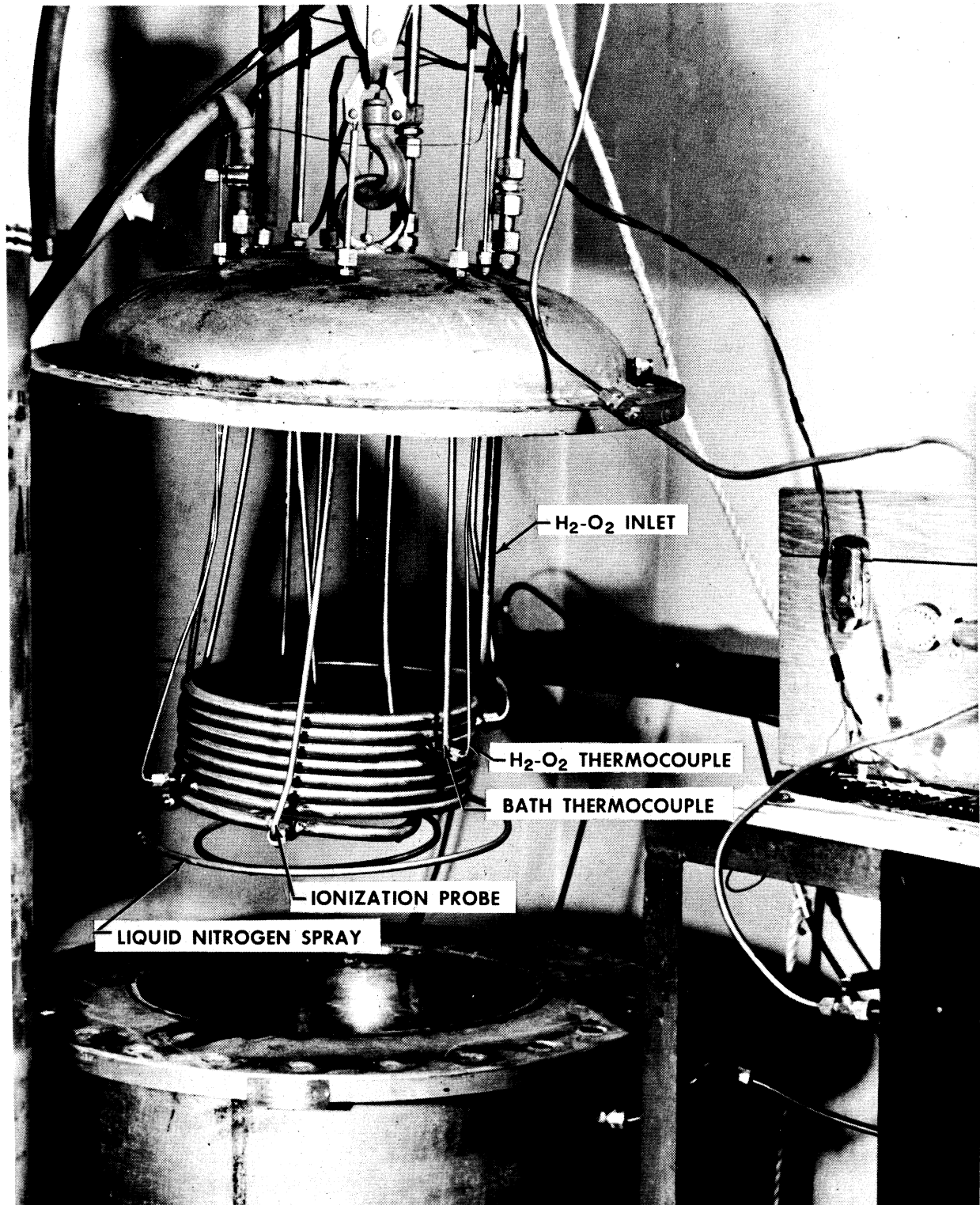


Figure 8. Photograph of the Coiled Detonation Tube and the Low-Temperature Vessel

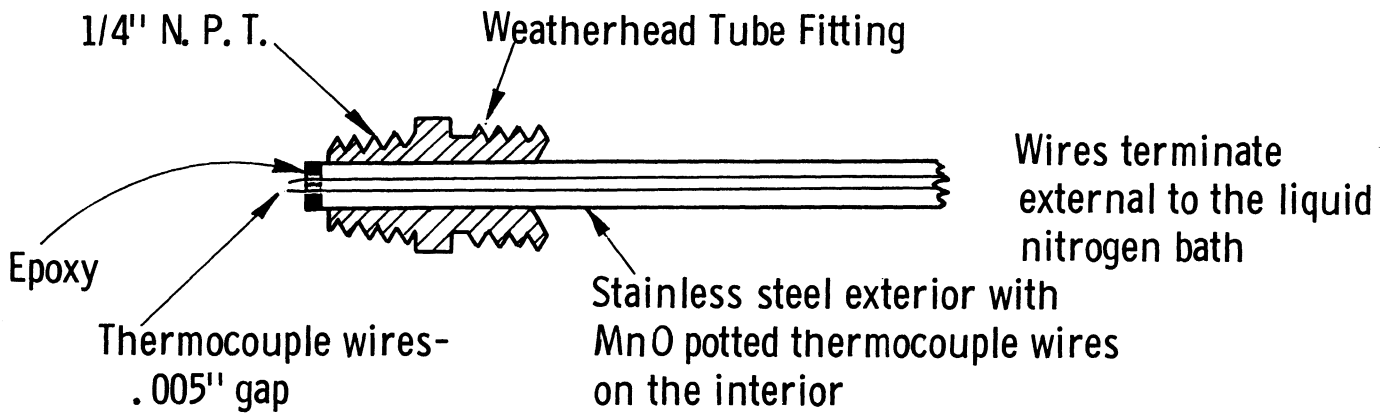


Figure 9. Schematic View of the Ionization Probe for Detonation Velocity Measurements

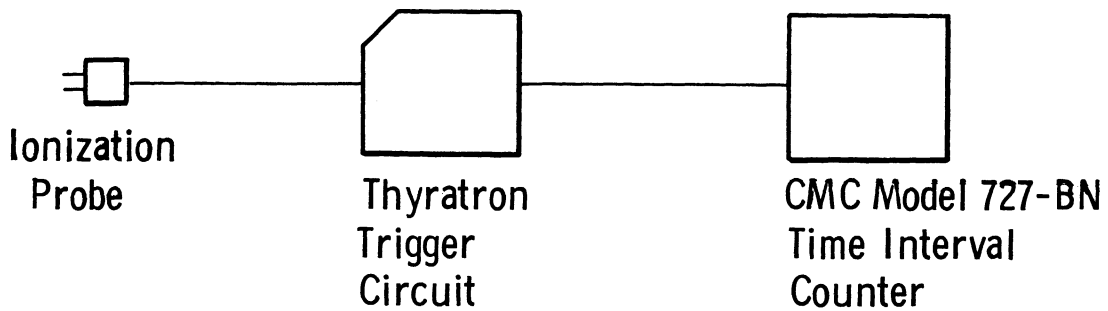


Figure 10. Schematic View of the System for Detonation Velocity Measurements



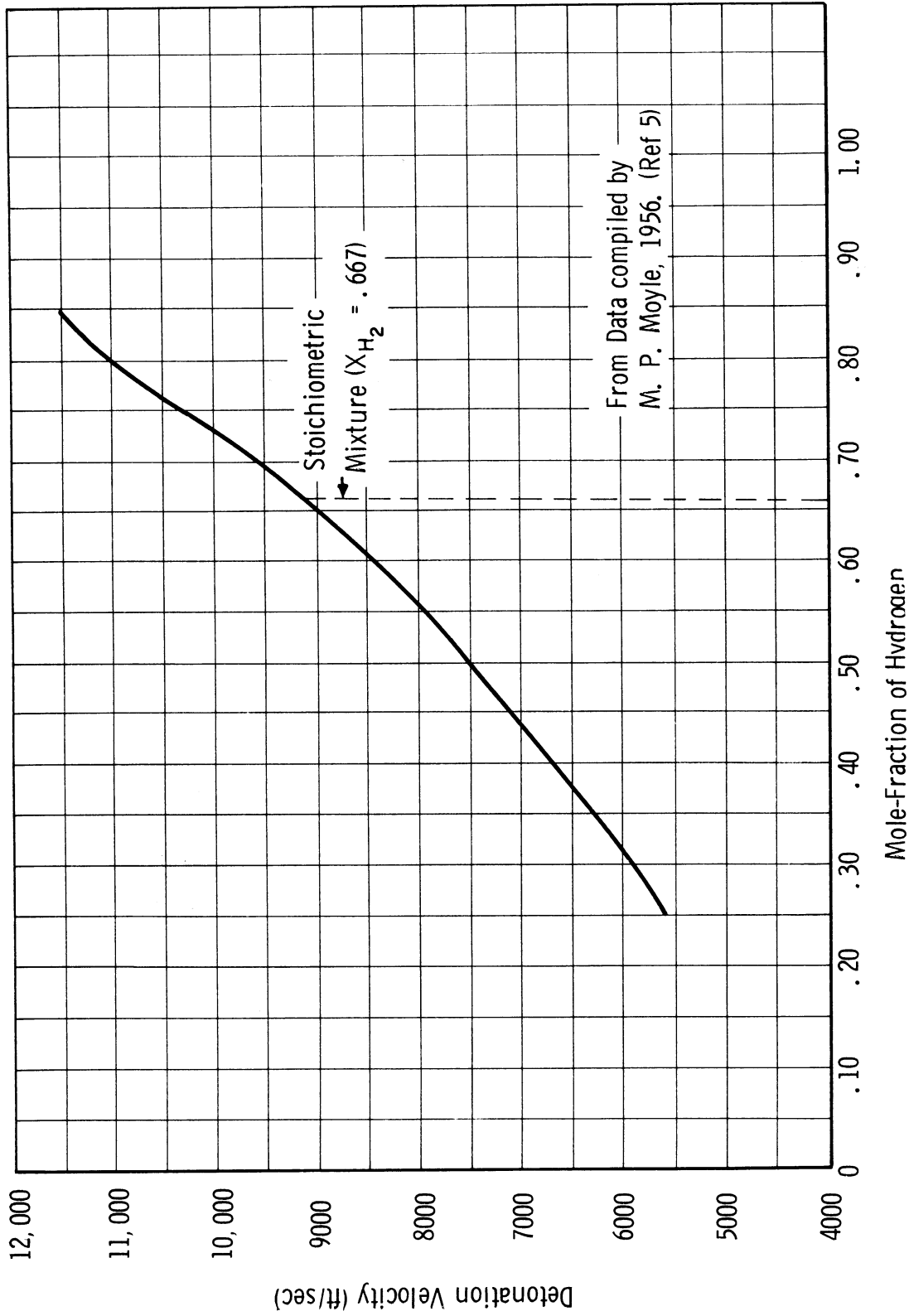


Figure 11. Experimental Detonation Velocity,  $U_D$ , of Hydrogen-Oxygen Detonations as a Function of the Mole-Fraction of Hydrogen ( $X_{H_2}$ ) from Data Obtained by Moyle (Reference 5)

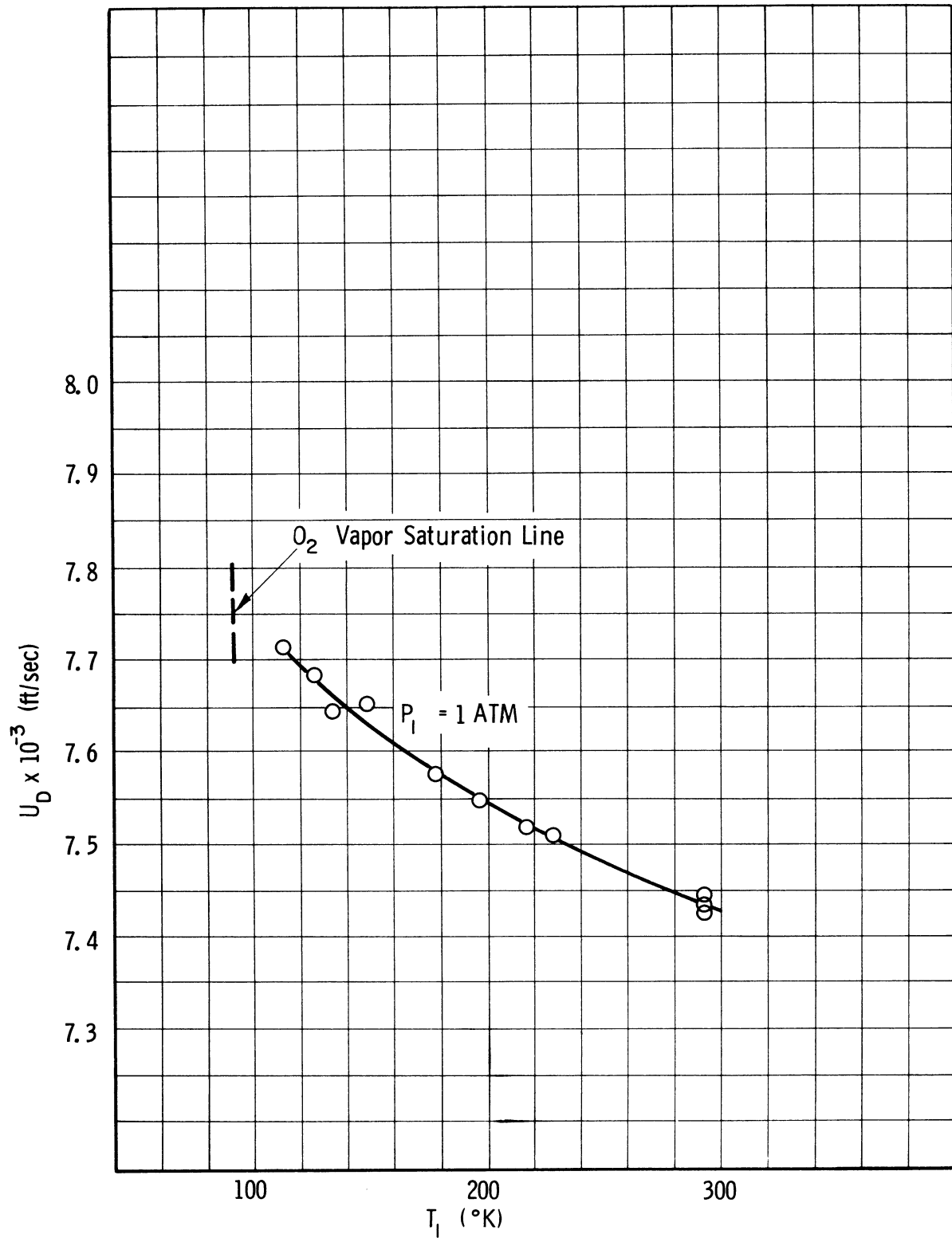


Figure 12. Experimental Detonation Velocity,  $U_D$ , of Hydrogen-Oxygen Detonations as a Function of the Initial Temperature,  $T_1$ , for  $X_{H_2} = 0.500$

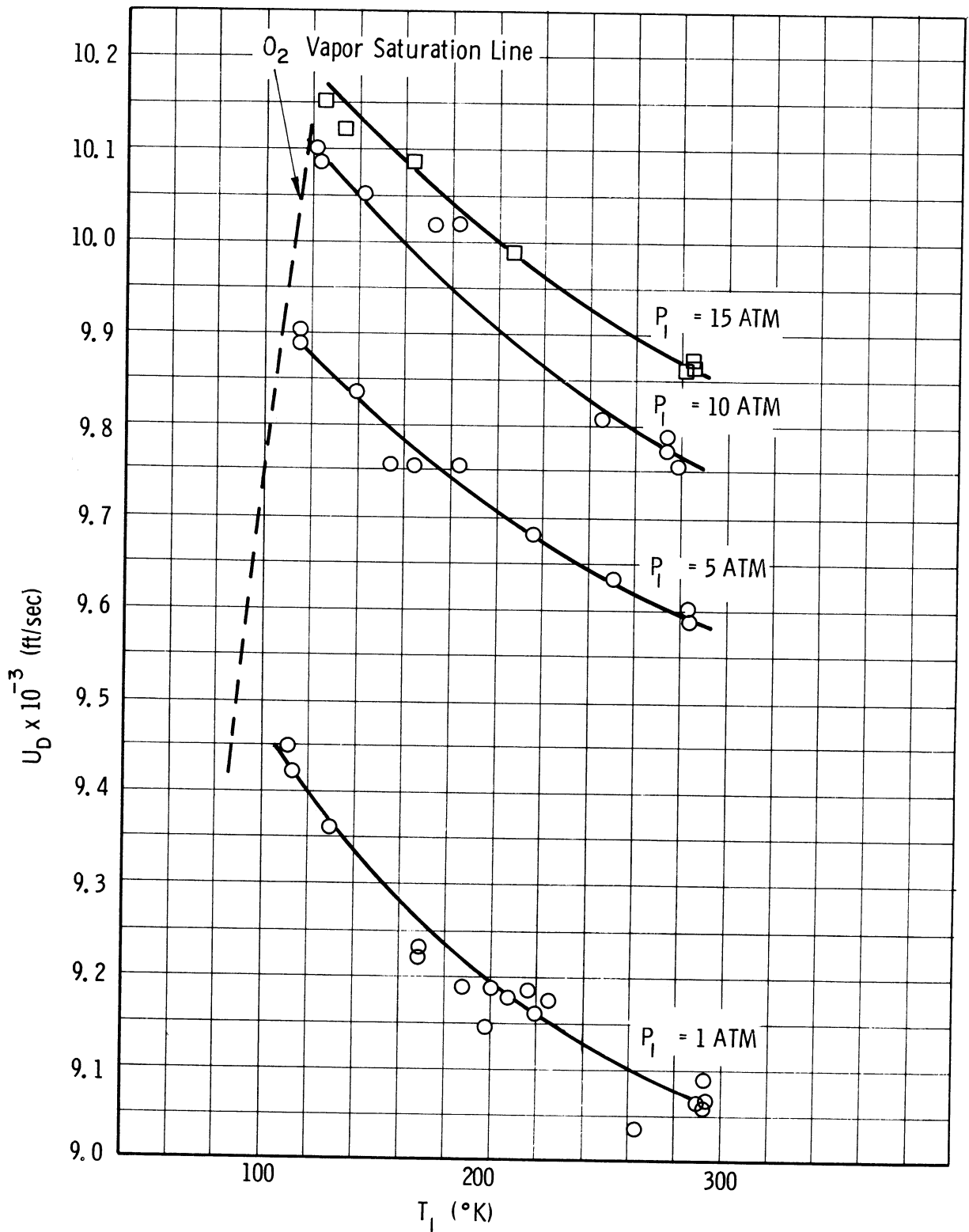


Figure 13. Experimental Detonation Velocity,  $U_D$ , of Hydrogen-Oxygen Detonations as a Function of the Initial Temperature,  $T_1$ , for  $X_{H_2} = 0.667$

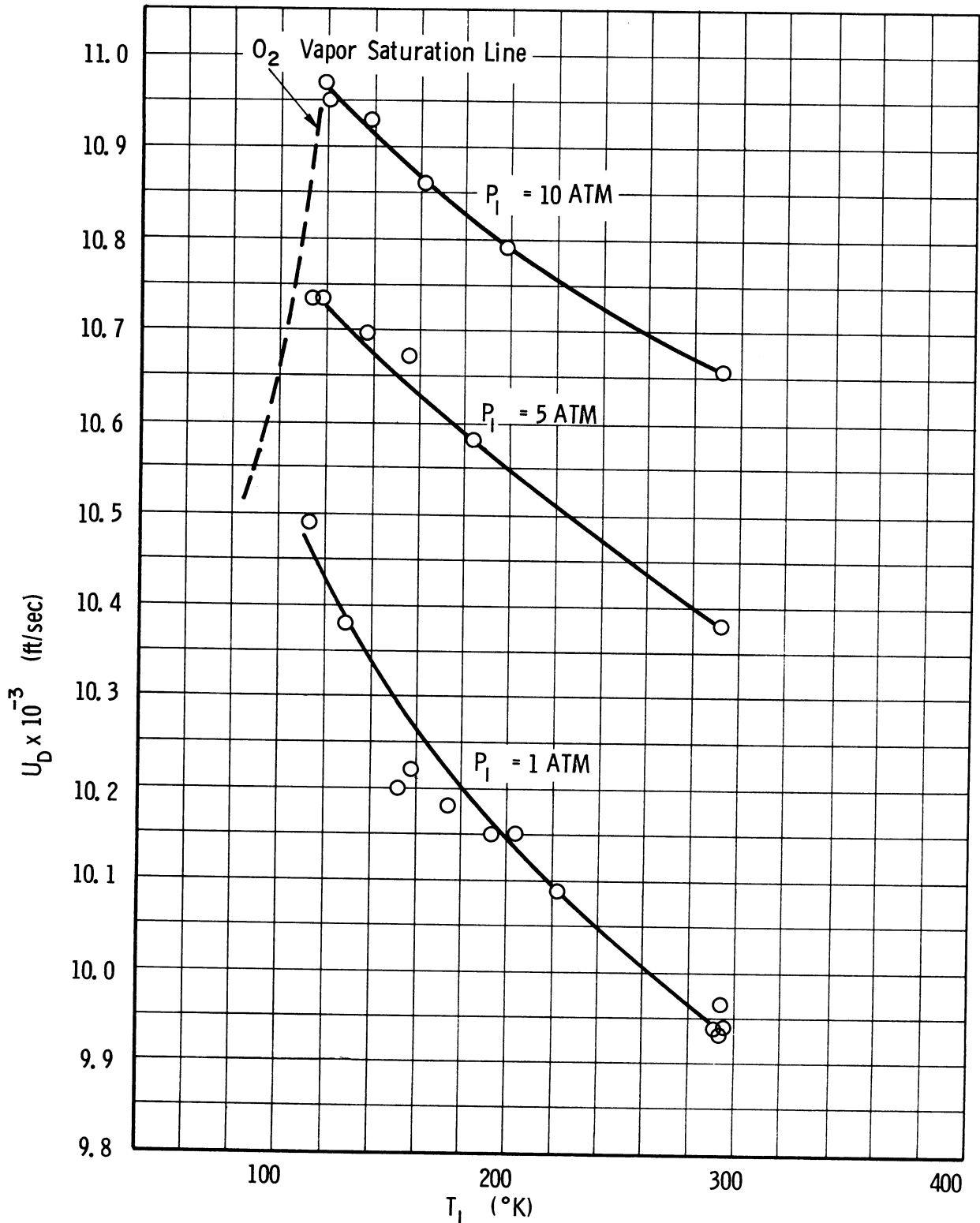


Figure 14. Experimental Detonation Velocity,  $U_D$ , of Hydrogen-Oxygen Detonations as a Function of the Initial Temperature,  $T_1$ , for  $X_{H_2} = 0.730$

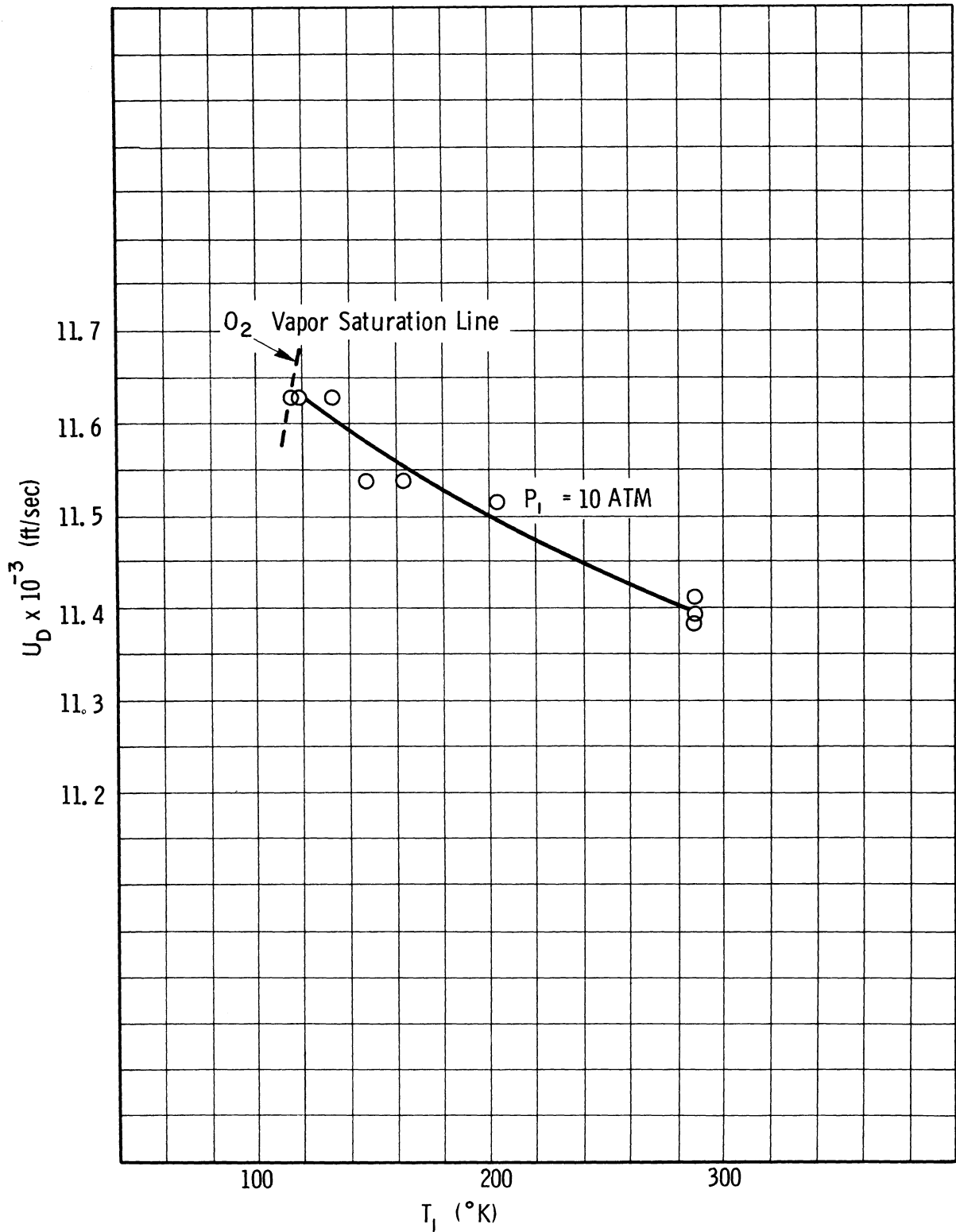


Figure 15. Experimental Detonation Velocity,  $U_D$ , of Hydrogen-Oxygen Detonations as a Function of the Initial Temperature,  $T_1$ , for  $X_{H_2} = 0.800$

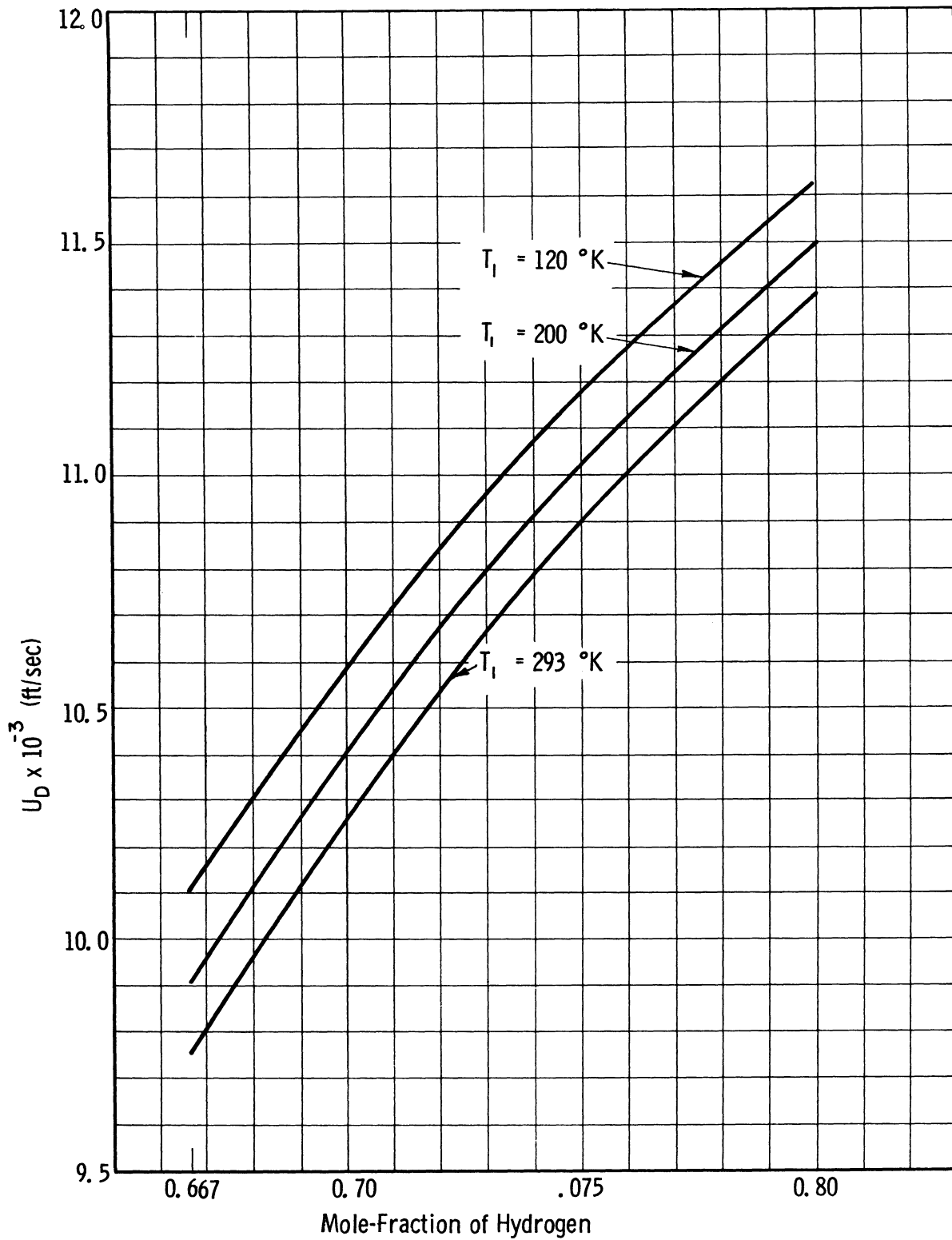


Figure 16. Experimental Detonation Velocity,  $U_D$ , of Hydrogen-Oxygen Detonations as a Function of the Mole-Fraction of Hydrogen,  $X_{H_2}$ , for Initial Pressure,  $P_1 = 10$  Atmospheres

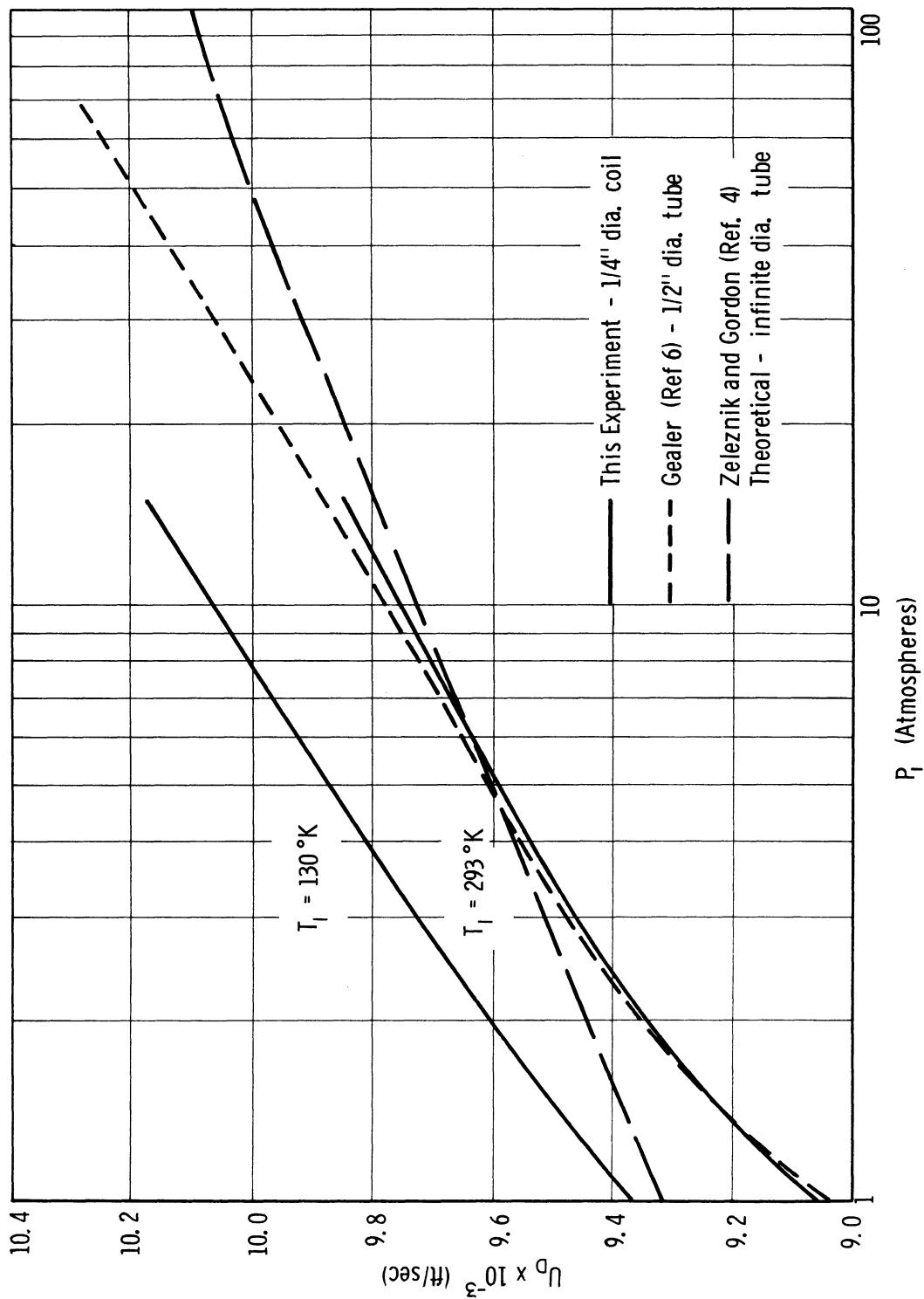


Figure 18. Comparison of Experimental Detonation Velocity,  $U_D$ , as a Function of the Log of the Initial Pressure,  $P_1$ , at Various Initial Temperatures,  $T_1$ , with the Results of Other Investigators for Stoichiometric ( $X_{H_2} = .667$ )  $H_2 - O_2$  Mixtures

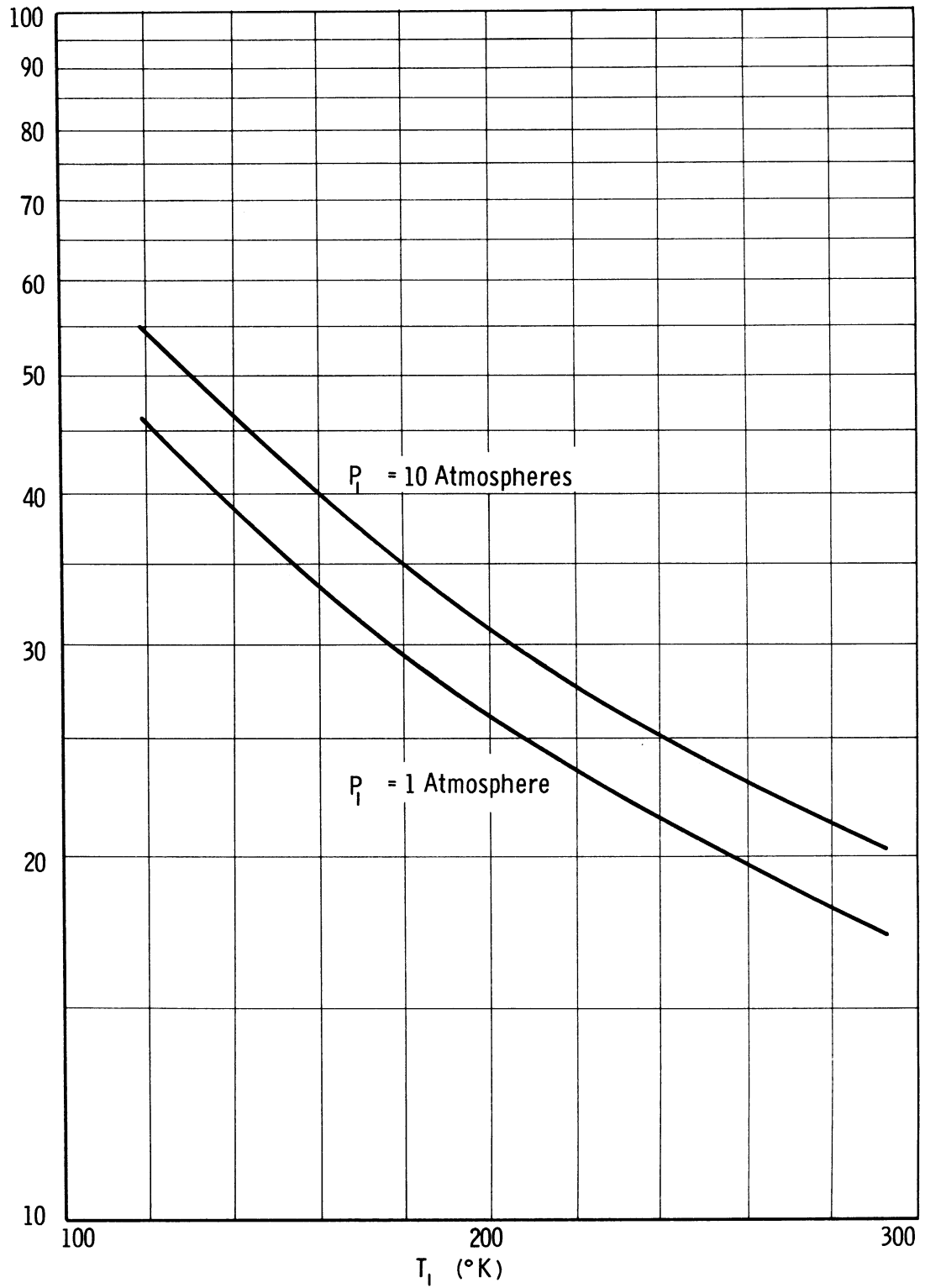


Figure 19. Log of the Detonation Pressure Ratio,  $P_2/P_1$  (obtained from experimental detonation velocity measurements) as a Function of the Initial Temperature,  $T_1$ , for Stoichiometric ( $X_{\text{H}_2} = .667$ )  $\text{H}_2 - \text{O}_2$  Mixtures



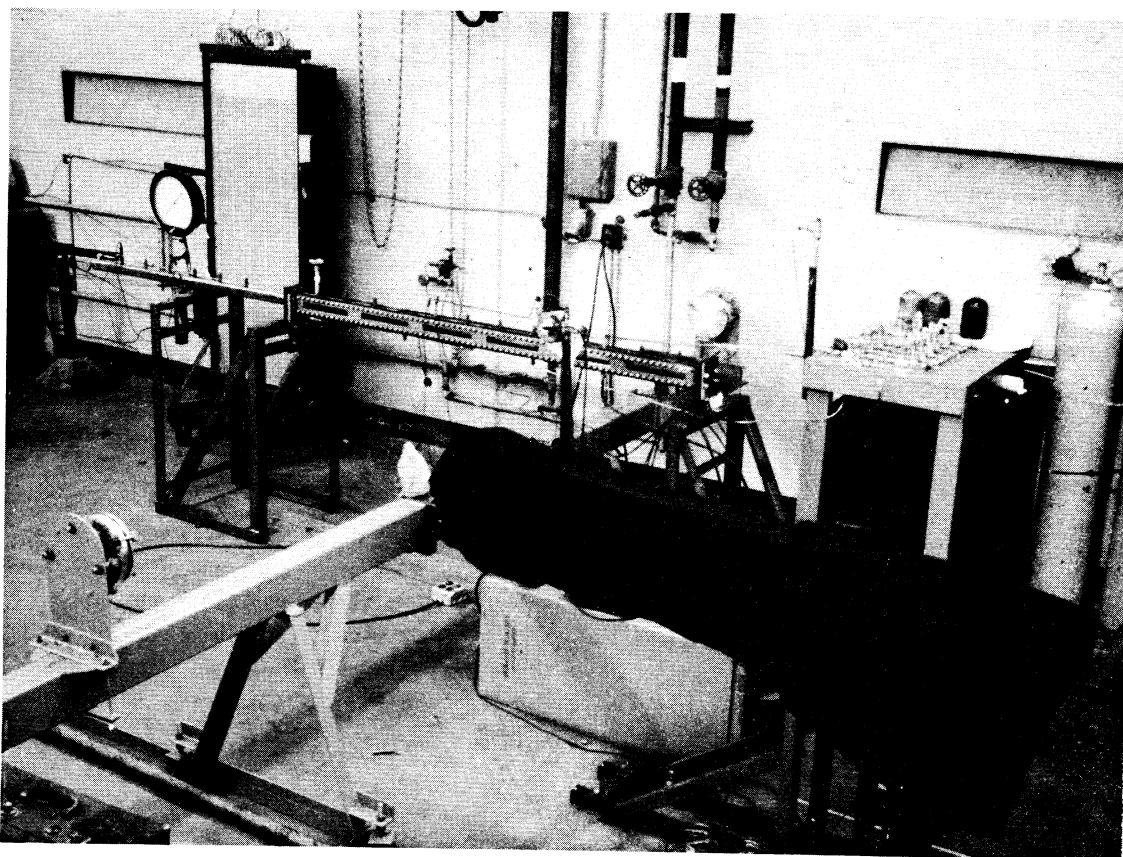


Figure 20. Photograph of the Test Setup for Detonation through Heterogeneous, Liquid-Gas Media

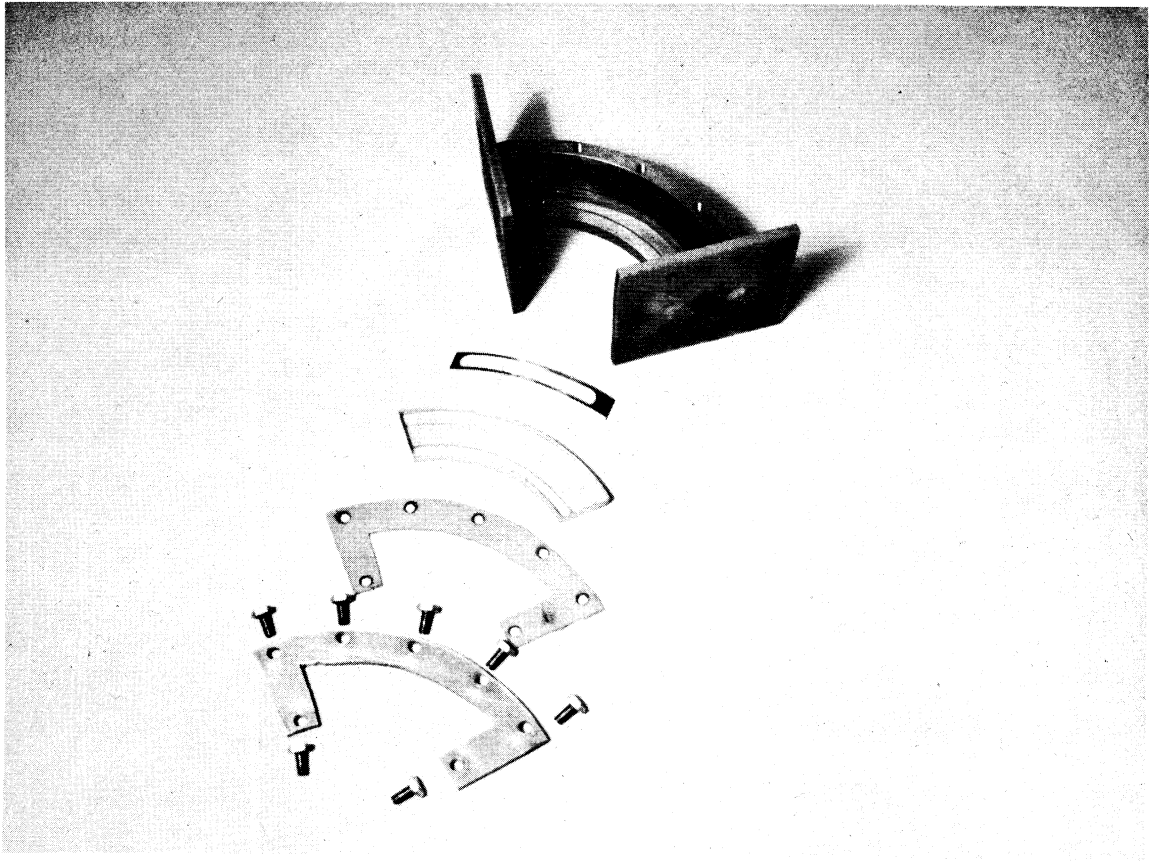


Figure 22. Exploded View of Circular Test Section with Provision for Two-Dimensional Pressure Relief in Radial-Inward Direction. (Note: From top of picture: test section, film holder, glasswindow, gasket, cover plate)

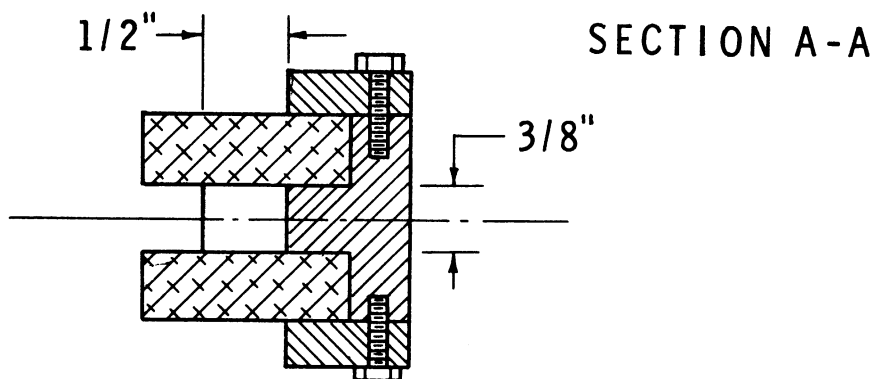
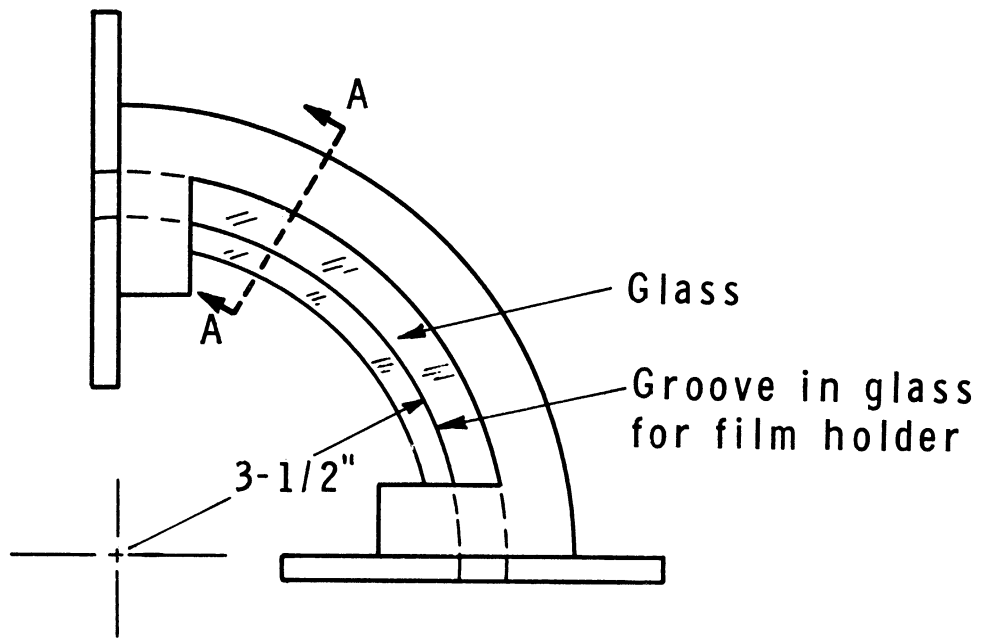
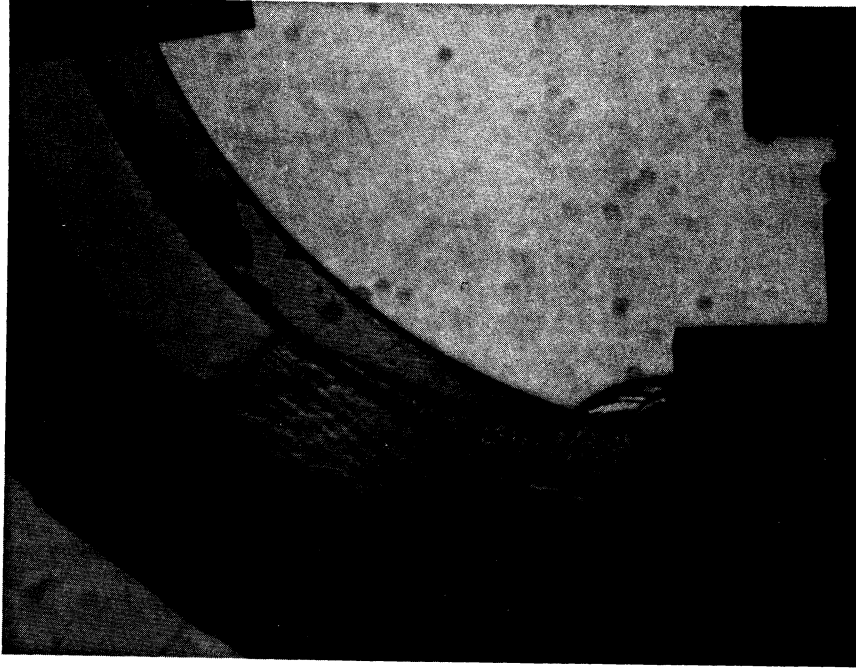


Figure 23. Schematic View of the Circular Test Section with Provision for Two-Dimensional Pressure Relief in Radial-Inward Direction



(a)



(b)

Figure 24. Schlieren Photographs of Stoichiometric, Hydrogen-Oxygen Detonation Waves in the Circular Test Section. (a) With radial-inward relief; (b) With steel wall on inner radius (no relief)

UNIVERSITY OF MICHIGAN



3 9015 02826 5844